[redacted]

NASA CR-54329
MND-3178

INVESTIGATION OF FUEL LOSS FROM TUNGSTEN-URANIUM DIOXIDE BODIES [U]

by

W. Precht and L. Sundquist

prepared for

NATIONAL AERONAUTICS AND SPACE ADMINISTRATION

Contract NAS 3-5217

MARTIN MARIETTA
NUCLEAR DIVISION Baltimore 3, Maryland

[redacted]

[redacted]

NASA CR-54329
MND-3178

FINAL REPORT

INVESTIGATION OF FUEL LOSS FROM TUNGSTEN-URANIUM DIOXIDE BODIES [U]

by

W. Precht and L. Sundquist

prepared for

NATIONAL AERONAUTICS AND SPACE ADMINISTRATION

November 30, 1964

Contract NAS 3-5217

Technical Management
NASA Lewis Research Center
Cleveland, Ohio
Materials and Structures Division
Gordon Watson

Q65-1413

[redacted] Group 1
Excl[redacted]uto-
mat[redacted]ng,

This document contains [redacted] defined [redacted] Atomic Energy Act [redacted] ittal or the [redacted] of its contents in any manner to an unauthorized [redacted] is prohibited.

MARTIN MARIETTA
NUCLEAR DIVISION Baltimore 3, Maryland

[redacted]

[redacted]

ABSTRACT

50004

High uranium dioxide losses have been experienced with various simulated fuel plates of tungsten-uranium dioxide during thermal cycle testing. Results of this study indicate that the use of fine particle uranium dioxide (< 1 micron) or uranium dioxide-yttrium oxide solid solution fuel particles greatly reduces this fuel loss. Simulated fuel plates containing these fuel forms have been successfully fabricated and tested. Fuel loss with these fuel forms is reduced approximately one order of magnitude. It is believed that fuel losses can be further minimized by incorporating a fine-particle fuel form made from a stabilized uranium dioxide. ~~Secret~~

Author

Conf. R.D.

[redacted]

SUMMARY

Recent studies at NASA-Lewis Research Center have shown high uranium dioxide fuel losses when simulated fuel plates of tungsten-uranium dioxide are exposed to high temperature thermal cycle tests.

This particular study was undertaken to determine the effect of stabilization of the uranium dioxide by solid solution synthesis and the use of very fine uranium dioxide particles on the fuel retention properties of fuel plates.

The solid solution particles (uranium dioxide-yttrium oxide, uranium dioxide-thorium dioxide) were prepared by intimately blending the powders, compacting the blend, granulating to the desired size and sintering these particles in hydrogen at 1700° C for 16 hours. Uranium dioxide particles were also prepared with surface coatings of the same additives used in forming the solid solution. The fuel loading of all test samples prepared was maintained at 20 volume percent uranium dioxide. In the case of additives, a maximum of 10 volume percent additive was used, with the result that a maximum of 30 volume percent total ceramic loading existed in these plates.

Fuel plates were prepared by cold compacting the core blend of tungsten powder uranium dioxide which were then sintered at 1725° C for 16 hours in hydrogen. The sintered cores were wrapped in 2.5-mil tungsten foil for cladding, and hot rolled at 1950° C to 2000° C to 50% reduction in thickness in 5% increments. The rolled samples were ~4 inches long, 1 inch wide and 0.020 inch thick. Test specimens of 1 x 1.5 x 0.020 inches were cut from these samples for fuel retention studies.

Fuel loss was determined by assuming that any weight change encountered during thermal testing was due to uranium dioxide loss. Test specimens were exposed to a thermal static test of 10 hours at 4500° F at 5×10^{-5} torr and a thermal cycle test of 10 cycles, of 30 minutes each, at a temperature of 4500° F at 5×10^{-5} torr. Fuel loss under static test conditions is believed to be primarily due to losses from the unclad edges of the samples. The major surfaces were clad with tungsten foil. The fuel loss encountered during cycle testing, however, is considered to be due to a partial dissociation or reduction of the uranium dioxide. The decomposition products, generated during the cycling, manage to escape through tungsten grain boundary paths as the test progresses.

Most effective in minimizing this fuel loss has been the use of fine-particle uranium dioxide and uranium dioxide stabilized in a solid

solution with yttria. The use of uranium dioxide-thorium dioxide solid solution particles or thorium dioxide-coated uranium dioxide particles exhibited a smaller effect on the reduction of fuel loss. Fuel retention under thermal cycle condition was improved by approximately one order of magnitude, within a 10-cycle span, with the use of the fine-particle uranium dioxide or the uranium dioxide-yttrium oxide solid solution. The best improvement in fuel retention resulted from the use of fine particle uranium dioxide fuel.

It was recommended that an evaluation be made of the use of the solid solution forms of uranium dioxide, fine-particle uranium dioxide in a particle range up to 10 microns, and a combination of stabilized uranium dioxide in the particle size range of 1 to 10 microns.

CONTENTS

I. INTRODUCTION

Tungsten-uranium dioxide composite fuel elements are under consideration at NASA for use in nuclear rocket applications. These fuel elements must be capable of operating at temperatures of at least 4500° F in flowing hydrogen under severe mechanical and thermal stresses.

Although it has been demonstrated that the components of the tungsten-uranium dioxide system are compatible to the melting point of uranium dioxide, excessive loss of the uranium dioxide from the fuel elements has been encountered during extended thermal cycle testing. The major factors which can effect uranium dioxide loss are considered to be (Ref. 1):

(1) Volatilization of exposed uranium dioxide particles.

(2) Interconnection of uranium dioxide particles (between internal and exposed particle).

(3) Diffusion of uranium dioxide through micropores and microcracks in the tungsten cladding.

(4) High local concentration of impurities in the uranium dioxide.

(5) Partial decomposition of the uranium dioxide.

(6) Differences in thermal expansion between tungsten and uranium dioxide.

The primary efforts of this study were directed towards restricting the volatilization and/or the partial decomposition of the uranium dioxide and minimizing the effect of the thermal expansion differences between the tungsten and the uranium dioxide. In addition, test fuel plates were fabricated to determine the effect of several process variables on fuel loss.

II. PROGRAM EFFORT

The program was divided into four specific tasks, which are listed below. Task I involved a comparison of the core fabrication process and hot rolling process as used at NASA-Lewis Research Center (Ref. 6) and Martin-Nuclear (Ref. 7). Task II covered variations in the standard core fabrication process. Task III involved a study of the effects of physical variations in the uranium dioxide particles with respect to particle size, shape, and density (hollow-core particles). These variables were introduced in an attempt to minimize the effect of the thermal expansion difference between tungsten and uranium dioxide. Modifications to the uranium dioxide, including solid solution additives, coatings applied to the uranium dioxide particles, and a coprecipitated oxide system were covered under Task IV. These modifications were made to the fuel in an attempt to reduce volatilization of the uranium dioxide and also to reduce or eliminate the decomposition or disproportionation of the uranium dioxide.

The variables studied under each task are summarized below:

(1) Task I

(a) Cermet cores were prepared for rolling and were delivered to NASA-Lewis Research Center for hot rolling.

(b) Cermet cores were prepared for rolling by NASA-Lewis Research Center and hot rolled by Martin-Nuclear.

(2) Task II

(a) Standard cores were surface ground prior to application of tungsten cladding and were subsequently hot rolled to a 50% reduction in thickness, using standard rolling procedures at a temperature of ~2000° C.

(b) Standard cores were hot rolled to a 50% reduction in thickness at a temperature of ~2400° C.

(3) Task III

The following physical variations of uranium dioxide were investigated to determine their effect on fuel loss:

(a) The use of 0.6-micron average diameter uranium dioxide particles.

(b) The use of hollow-core uranium dioxide particles of 30- to 60-micron diameter.

(c) The use of uranium dioxide particles of 30- to 60-micron particle size produced by agglomerating fine-particle (0.6-micron) uranium dioxide.

(4) Task IV

The following physical and/or chemical modifications were investigated to determine their effects on the high temperature stability of the fuel:

(a) Solid solution of uranium dioxide with yttrium oxide (Y_2O_3).

(b) Solid solution of uranium dioxide with thorium dioxide (ThO_2).

(c) A fuel mixture produced by coprecipitating yttrium-uranium (+6) oxides.

(d) Coating of uranium dioxide particles with thorium dioxide (ThO_2).

(e) Coating of uranium dioxide particles with yttrium oxide (Y_2O_3).

(f) Coating of uranium dioxide particles with thoriated tungsten.

(g) Coating of uranium dioxide particles with a duplex* coating of tungsten and thorium dioxide (ThO_2).

The following modifications were made in addition to the above:

(a) The use of hollow-core uranium dioxide particles incorporated into a tungsten matrix and densified by sintering but not by hot working.

(b) The use of fine-particle uranium dioxide blended with tungsten powder, formed, and sintered into particles of ~50-micron size.

---

*The duplex coating or double layer coating technique is described in the Materials Preparation section, Paragraph 9, of this report.

(c) Similar to Task IV, Phase (f), but with a different amount of thorium dioxide in the thoriated tungsten coating.

The materials and process used for the fabrication of a standard fuel plate are described in the appropriate section of this report. The fuel retention properties of the modifications investigated under this program are compared to the standard Martin fuel plate. The test fuel plates processed in this study all contained a fuel loading of 20 volume percent uranium dioxide. When additions were made to the uranium dioxide, they were restricted to a maximum of 10 volume percent of the core, so that a fuel plate with additives would always contain at least 70 volume percent tungsten.

III. EXPERIMENTAL PROCEDURES

A. RAW MATERIALS

Three types of uranium dioxide were used in this study. The uranium dioxide used for the standard plates, Task I, Task II, and several phases of Task IV was standard spherical-particle uranium dioxide, as supplied by Nuclear Materials and Equipment Corporation (NUMEC), which has a particle size of -270 + 400 mesh (37 to 53 microns) with a maximum impurity level of < 300 ppm. The chemical analysis of this material is shown in Table 1.

Two lots of depleted, ceramic grade uranium dioxide powder, each having an average particle size of 0.6 micron, as determined by Fisher subsieve sizer measurement, were used. The chemical analyses of these powders are given in Tables 2 and 3. Lot 4E-5297 is hereafter referred to as the low fluorine ceramic grade uranium dioxide, while Lot S-4209 is referred to as the high fluorine material because the most significant difference between these powders was the fluorine content. These powders were used directly in the fabrication of Task III, Phase (a) fuel plate test samples. The uranium dioxide containing the low fluorine was also used in the preparation of the solid solution particles, the agglomerated particles, and the hollow-core particles.

The yttrium oxide and thorium dioxide used for particle coating and solid solution additions were supplied by American Potash and Chemical Corporation. The analyses of these materials are shown in Tables 4 and 5.

The tungsten trioxide powder used for particle coating was prepared by oxidizing General Electric Company 0.88-micron size tungsten powder at 650° C in air. This tungsten powder was also used as the matrix material in the fabrication of the cermet core. Table 6 shows the chemical analysis of the tungsten powder. The tungsten foil used as clad material was purchased from the Rembar Company.

B. MATERIALS PREPARATION

1. Hollow-Core Spherical Uranium Dioxide Particle

Low-fluorine uranium dioxide powder was heated in air for one hour at 900° C to form U_3O_8. The U_3O_8 powder was processed into -270 + 400 mesh hollow uranium dioxide spheres in the following manner:

TABLE 1

Chemical Analysis of NUMEC Spherical UO_2--NUMEC Lot 3E-0247

Tasks I and II

Element	Analysis (ppm)
Fe	<10
B	<0.5
Co	<5
Cd	<0.5
Mn	<10
Al	60
M	<10
Zn	<10
Sn	<2
Cu	<6
Pb	<2
Cr	<10
Si	<25
Ti	<10
Ni	<10
Mo	20
V	<1
Zr	10
Be	<1
Ca	<20
In	<2
Sb	<1
Bi	<1
P	<50
Au	<10
Na	<20

Sieve analysis
+ 200: 0.15%
- 200 + 270: 0.99%
- 270 + 325: 79.01%
- 325 + 400: 18.99%
- 400: 0.86%

Major to minor axis 1:1 to 2:1--100%

TABLE 2

Chemical Analysis of Ceramic Grade UO_2

(NUMEC Lot S-4209)

Element	Analysis (ppm)
Fe	40
B	0.5
Co	5
Cd	0.5
Mn	10
Al	20

TABLE 2 (continued)

Element	Analysis (ppm)
Mg	10
Zn	2
Cu	6
Cr	10
Si	50
Ti	10
Ni	20
Mo	25
F	790

Average particle size by Fisher subsieve sizer = 0.61 micron
Surface area (BET) = 2.75 m^2/gm

TABLE 3

Chemical Analysis of Ceramic Grade UO_2 (Nuclear Fuel Services, Inc. Lot 4E-5297

Element	Analysis (ppm)
Ag	0.10
Al	2
B	0.20
Ba	5
Be	0.10
Bi	1
Ca	18
Cd	0.10
Co	5
Cr	5
Cu	2
Fe	15
Mg	4
Mn	2
Mo	1
Na	40
Ni	23
P	10
Pb	1
Sb	1
Si	15
Sn	1
Ti	1

TABLE 3 (continued)

Element	Analysis (ppm)
V	2.5
Zn	25
Zr	2
F	139

Particle size = 0.61 micron (by Fisher subsieve sizer)
Bulk density = 0.89 g/cm^3
O/U = 2.07
% U = 87.70

TABLE 4

Chemical Analysis of Y_2O_3

Element/Compound	Analysis (ppm)
Gadolinium oxide	Not detected
Neodymium oxide	Not detected
Dysprosium oxide	Not detected
Holmium oxide	Not detected
Erbium oxide	Not detected
Calcium	112
Silicon	35
Loss on ignition	0.39%

Particle size by Fisher subsieve sizer = 1.5 microns

TABLE 5

Chemical Analysis of ThO_2 Powder

Element/Compound	Analysis (ppm)
Rare earth oxides	20
Fe_2O_3	4.45
Loss on ignition	Nil
Particle size (by Fisher subsieve sizer)	0.55 micron

(1) The powder was pressed into 1-inch diameter pellets at 30 tons per square inch (tsi) and then hand crushed into approximately 1/16-inch pieces. These pieces were then granulated in screens placed in a Ro-Tap Sieve Shaker in which steel balls were used to facilitate granulation.

(2) These granules (-230 + 325 mesh) were then spheroidized by passing them through an oxyacetylene flame. The spheroidized particles were collected and reduced to uranium dioxide by heating in hydrogen at 1150° C for two hours.

(3) Spherical uranium dioxide particles produced in this way exhibit central porosity due to the release and accumulation of oxygen during the spheroidizing process.

(4) The -270 + 400 mesh fraction of this material was separated and used in the fabrication of Task III, Phase (b) and Task IV, Phase (h) fuel plate test samples. A photomicrograph of this material is shown in Fig. 1a.

TABLE 6

Chemical Analysis of Tungsten Powder
Lot U.O. 88-4436

Element	Analysis (ppm)
Al	6
Ca	27
Si	<7
Mo	<15
Fe	35
Cr	<6
Ni	24
Cu	3
Mn	6
Mg	8
Sn	13
O	1100
C	15

Particle size by Fisher subsieve sizer = 0.91 micron

2. Agglomerated Fine-Particle Uranium Dioxide (ceramic grade)

The low fluorine content uranium dioxide powder used in Task III, Phase (a) was hand blended with a 2% poly-vinyl-alcohol-acetone

[redacted]

solution. The uranium dioxide binder blend was oven dried at 80° C. This powder was then processed into -270 + 400 mesh granules by the same granulation procedure as discussed in the preceding section.

These granules were used in the fabrication of Task III, Phase (c) fuel plate test samples.

3. Uranium Dioxide-Yttrium Oxide Solid Solution Particle

A uranium dioxide-yttrium oxide solid solution composition of uranium dioxide with 33 volume percent yttrium oxide (equivalent to 10 volume percent addition of yttrium oxide to the core) was prepared by wet blending the yttrium oxide and fine-particle uranium dioxide. The wet blend was then filtered, dried, and processed into granules. The granules were heat treated in hydrogen at 1700° C for 16 hours to form the solid solution. These particles were then used in the fabrication of the Task IV, Phase (a) fuel plate specimens. A photomicrograph of the material is shown in Fig. 1b.

4. Uranium Dioxide-Thorium Dioxide Solid Solution Particles

A uranium dioxide-thorium dioxide solid solution composition was prepared in the same manner as the uranium dioxide-yttrium oxide solid solution. The composition of the solid solution was uranium dioxide with 33 volume percent thorium dioxide (equivalent to 10 volume percent addition of thorium dioxide to the fuel core). This material was used in the fabrication of Task IV, Phase (b) fuel plate test samples. A photomicrograph of this material is shown in Fig. 2a.

5. Coprecipitated Uranium Dioxide-Yttrium Oxide

Fine-particle uranium dioxide-yttrium oxide in the proportions of 67 volume percent uranium dioxide-33 volume percent yttrium oxide were dissolved in nitric acid. This is equivalent to the uranium dioxide-33 volume percent yttrium oxide composition. A mixture of ammonium di-uranate and yttrium hydroxide was then coprecipitated by the addition of ammonium hydroxide. The mixture, after filtering and drying, was decomposed by heating in vacuum at 800° C for 16 hours to form a uranium dioxide-uranium trioxide-yttrium oxide complex. This complex was then processed into granules and sintered in vacuum at 1700° C for 16 hours. These particles were used in the fabrication of Task IV, Phase (c) fuel plate test samples. A photomicrograph of this material is shown in Fig. 2b.

6. Thorium Dioxide-Coated Spherical UO_2

Thorium dioxide was prepared for spray coating by blending with a water-alcohol mix, a dispersant (Darvan No. 7), and a binder (poly-vinyl

[redacted]

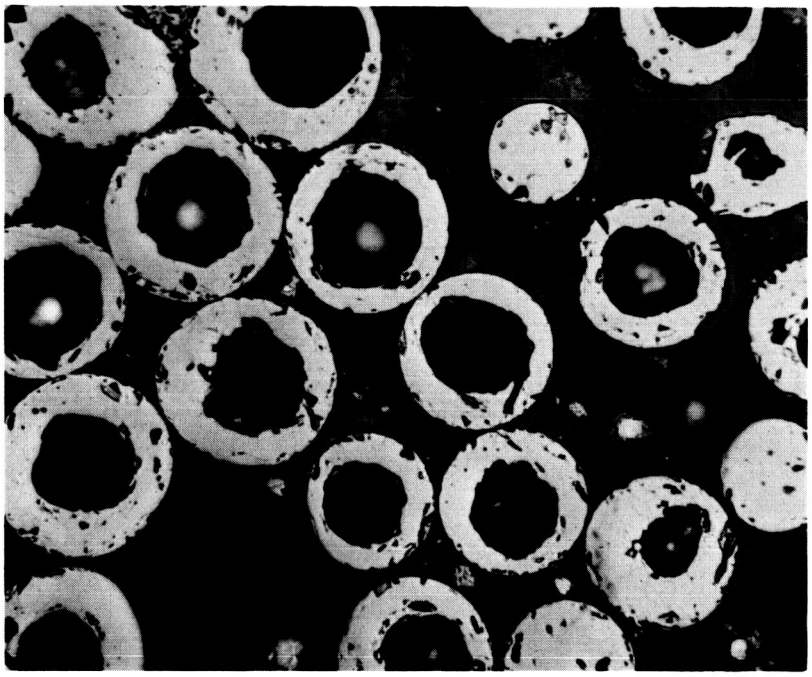

Magn 500X

Fig. 1(a). Hollow-Core Spherical Uranium Dioxide Particles, -270 + 400 Mesh

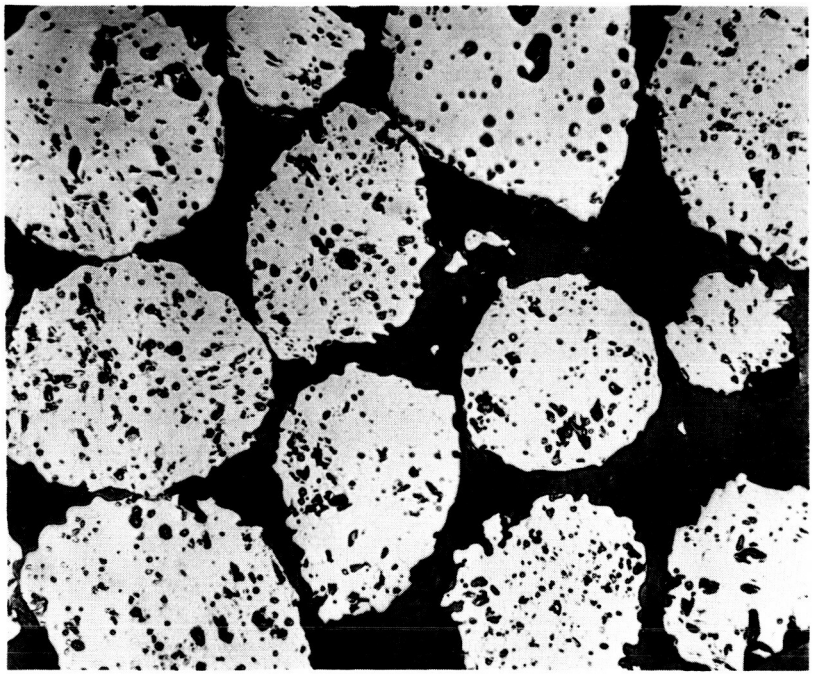

Magn 500X

Fig. 1(b). Uranium Dioxide-Yttrium Oxide Solid Solution Particles Containing 33 Volume Percent Yttrium Oxide, -270 + 400 Mesh

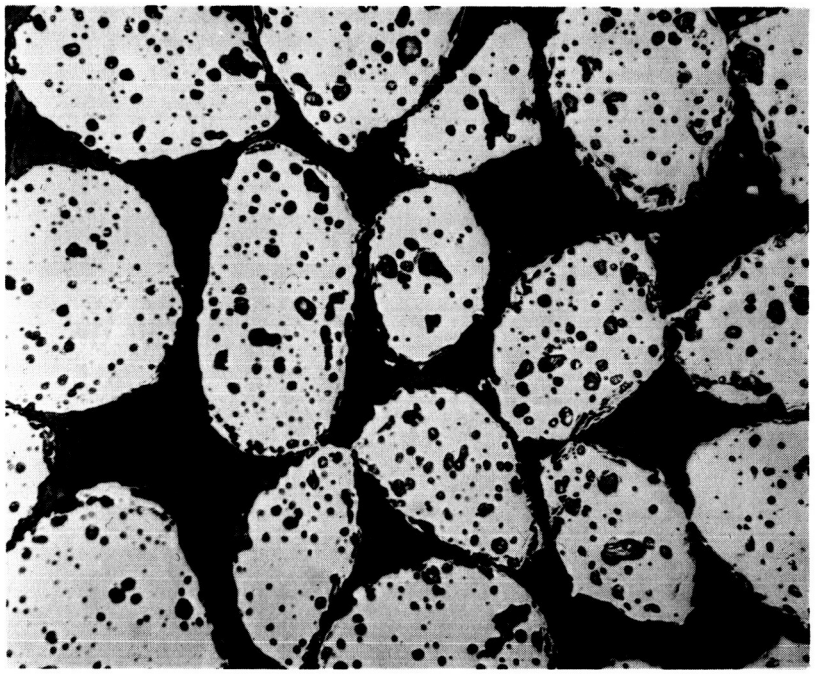

Magn 500X

Fig. 2(a). Uranium Dioxide-Thorium Dioxide Solid Solution Particles Containing 33 Volume Percent Thorium Dioxide, -270 + 400 Mesh

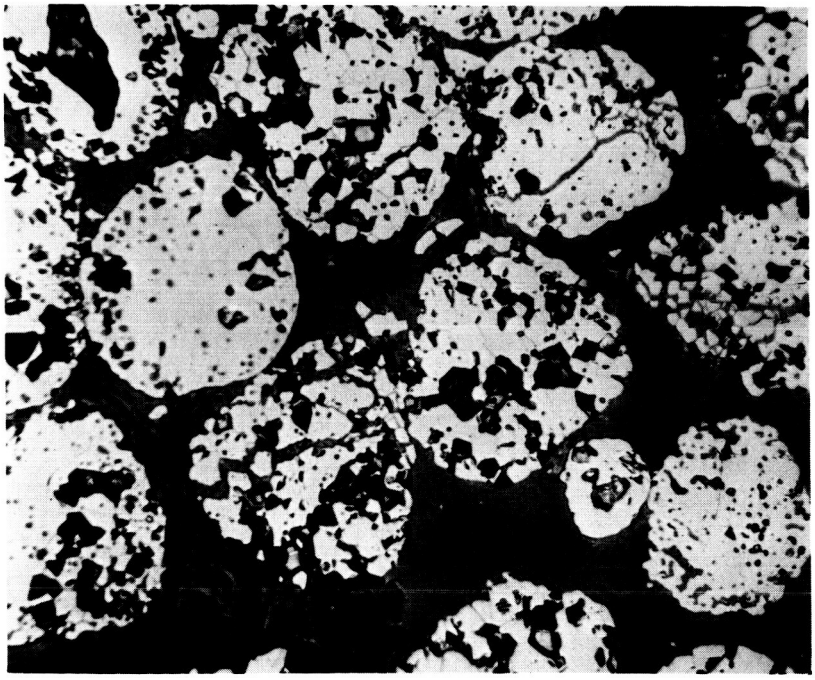

Magn 500X

Fig. 2(b). Uranium Dioxide-Yttrium Oxide Solid Solution Particles Containing 33 Volume Percent Yttrium Oxide, Prepared by a Coprecipitation Process -270 + 400 Mesh

alcohol). This blend was then used to deposit a thorium dioxide coating on the standard -270 + 400 mesh spherical uranium dioxide particles. The coating operation was accomplished in a 36-inch diameter, open-end drum which is rotated at approximately 2 rpm. The drum is heated, while rotating, by eight 375-watt heat lamps to allow the spray-coated uranium dioxide particles to dry rapidly. A wide, V-shaped baffle along the inside length of the drum collects the powder after each spraying and pours the powder onto an 8-inch diameter vibrating screen which contains metal pins on the screen surface. The metal pins help to separate particles which may have agglomerated during the spray coating. The uranium dioxide particles are coated as they are passing through the screen. Deposition was continued until a composition of uranium dioxide-33.3 volume percent thorium dioxide had been achieved. The thorium dioxide coated uranium dioxide particles were heat treated for 16 hours at 1700° C in hydrogen to densify the coating. It was realized that there would be a tendency for interdiffusion between the thorium dioxide coating and the uranium dioxide particle, probably resulting in the eventual dissolution by the uranium dioxide of the thorium dioxide coating, but the rate at which this reaction would proceed was not known. It was therefore expected that the behavior of this material during thermal cycling would approximate that of the uranium dioxide-thorium dioxide solid solution particles. These particles were used in the preparation of Task IV, Phase (d) fuel plate test samples. A photomicrograph of this material shown in Fig. 3a.

7. Yttrium Oxide-Coated, Spherical Uranium Dioxide

Yttrium oxide was prepared for spray coating in the same manner as discussed in the preceding section. This blend was then used to deposit an yttrium oxide coating on the standard -270 + 400 mesh, spherical uranium dioxide particles. Deposition was continued until a composition equal to uranium dioxide with 33 volume percent yttrium oxide had been achieved.

The yttrium oxide-coated uranium dioxide particles were heat treated for 16 hours at 1700° C in hydrogen to densify the coating. It was realized here, as in the case of thorium dioxide, that there would be a tendency for interdiffusion between the coating and the uranium dioxide particle but, again, the rate at which this reaction would proceed was not known. It was also expected that the thermal cycling behavior of this material would approximate that of the uranium dioxide-yttrium oxide solid solution particles. This material was used in the fabrication of Task IV, Phase (e) fuel plate test samples. Figure 3b shows the microstructure of this material.

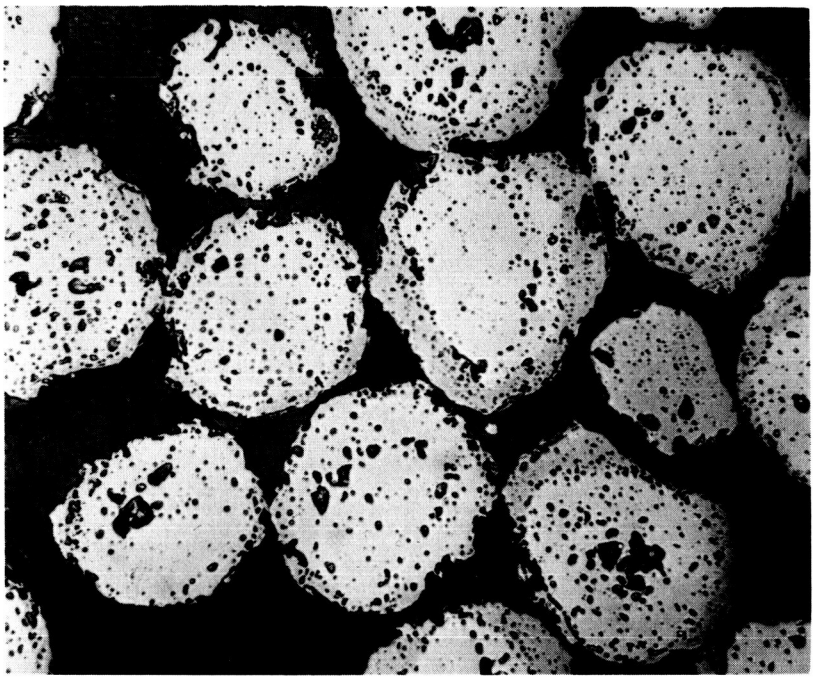

Magn 500X

Fig. 3(a). Thorium Dioxide-Coated Spherical, -270 + 400 Mesh, Uranium Dioxide Particles Containing 33 Volume Percent Thorium Dioxide

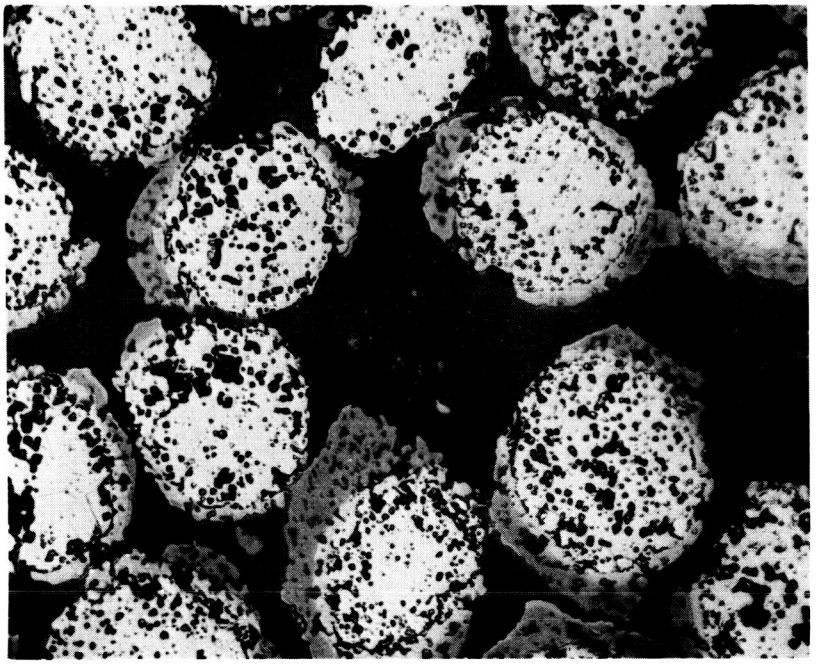

Magn 500X

Fig. 3(b). Yttrium Oxide-Coated Spherical, -270 + 400 Mesh, Uranium Dioxide Particles Containing 33 Volume Percent Yttrium Oxide

8. Thoriated Tungsten-Coated, Spherical Uranium Dioxide

The coating of spherical uranium dioxide with thoriated tungsten was accomplished by the codeposition of tungsten trioxide and thorium dioxide on uranium dioxide particles and subsequent hydrogen reduction of the codeposited mixture to thoriated tungsten. Blends were prepared for coating by blending appropriate quantities of tungsten trioxide and thorium dioxide with a suitable deflocculant (Darvan 7) and binders (poly-vinyl-alcohol). This blend was then spray coated onto the surfaces of -270 + 400 mesh, spherical uranium dioxide particles until the required coating weight was attained. Two coating compositions were prepared: one with 2 volume percent thorium dioxide in tungsten and the other with 4 volume percent thorium dioxide in tungsten. The particles were coated so that their composition was 60 weight percent uranium dioxide-40 weight percent coating. Figure 4a shows a cross section of the tungsten-2 volume percent thorium dioxide-coated uranium dioxide particles.

The tungsten trioxide-thorium dioxide-coated uranium dioxide particles were heat treated in hydrogen for two hours at 800° C, followed by two hours at 1160° C. It was necessary to heat treat the particles coated with the tungsten-4 volume percent thorium dioxide for an additional two hours at 1700° C to obtain a coherent coating. It is believed that this was due to the relatively large quantity of thorium dioxide in the coating.

These particles were used in the preparation of Task IV, Phase (f) and Task IV, Phase (j) fuel plate test samples.

9. Duplex Coating of Tungsten and Thorium Dioxide on Spherical Uranium Dioxide

The tungsten-thorium dioxide duplex coating on -270 + 400 mesh, spherical uranium dioxide was accomplished in two steps. First, a tungsten coating was applied to the particles by the deposition and subsequent hydrogen reduction of tungsten trioxide. The same process discussed in the previous section was used, except, of course, no thorium dioxide was added to the coating blend. Thorium dioxide coating was then deposited over the tungsten coating.

The composition of the tungsten-coated uranium dioxide spheres was 40 weight percent tungsten-60 weight percent uranium dioxide. A thorium dioxide coating was deposited over the tungsten coating until the amount of thorium dioxide relative to uranium dioxide was the same as in the uranium dioxide-thorium dioxide solid solution particles and in the thorium dioxide-coated uranium dioxide.

This material was used in the fabrication of Task IV, Phase (g) fuel plate test samples. Figure 4b shows the microstructure of this material as fired.

10. Dispersed Uranium Dioxide-Tungsten Sintered Particles

Fine-particle uranium dioxide was blended with tungsten powder in the ratio of 70 volume percent uranium dioxide-30 volume percent tungsten. The material was then dry blended, sieved, and compacted into pellets. The pellets were crushed and screened to yield -270 + 325 mesh particles. The particles were sintered in hydrogen for 16 hours at 1700° C. These fuel particles were used in Task IV, Phase (i).

C. ANALYTICAL VERIFICATION OF SOLID SOLUTION SYNTHESIS

The extent of solid solution of the uranium dioxide-yttrium oxide, uranium dioxide-thorium dioxide and coprecipitated uranium oxide-yttrium oxide compositions after the high temperature heat treatment was determined by X-ray diffraction. In all cases, complete solid solution of the two constituents of each system was shown.

The uranium dioxide-thorium dioxide solid solution has the cubic lattice assumed by uranium dioxide, with no evidence of a second phase (Ref. 2). This is predictable, since the experimental cation diameters of thorium and uranium differ by only about 5%. A substitutional type of solid solution could be expected in all ranges of concentration.

In the case of uranium dioxide-yttrium oxide, although yttrium and uranium differ greatly in nuclear mass and charge, the experimental diameters of the cations (Y^{+3}, U^{+4}) differ only by approximately 5%. Again, a solid solution of the uranium dioxide structure would be expected. A cubic phase was found for the uranium dioxide-yttrium oxide, which is in agreement with Barrington and Kerrs's $U_{1-x}O_2$, where the smaller lattice spacings are attributed to partial oxidation of U^{+4} to U^{+6} (Ref. 3). The patterns exhibited only the one phase, with one extraneous line attributed to a "super-lattice" effect in the solid solution. This effect was found in both of the solid solutions and is an "ordering effect" independent of the approach to solution.

Polarographic determinations of the O/U ratio were made on the uranium dioxide-yttrium oxide and uranium dioxide-thorium dioxide solid solution particles. A comparison was made of the O/U ratio of a U_3O_8 standard material with and without the yttrium oxide or thorium

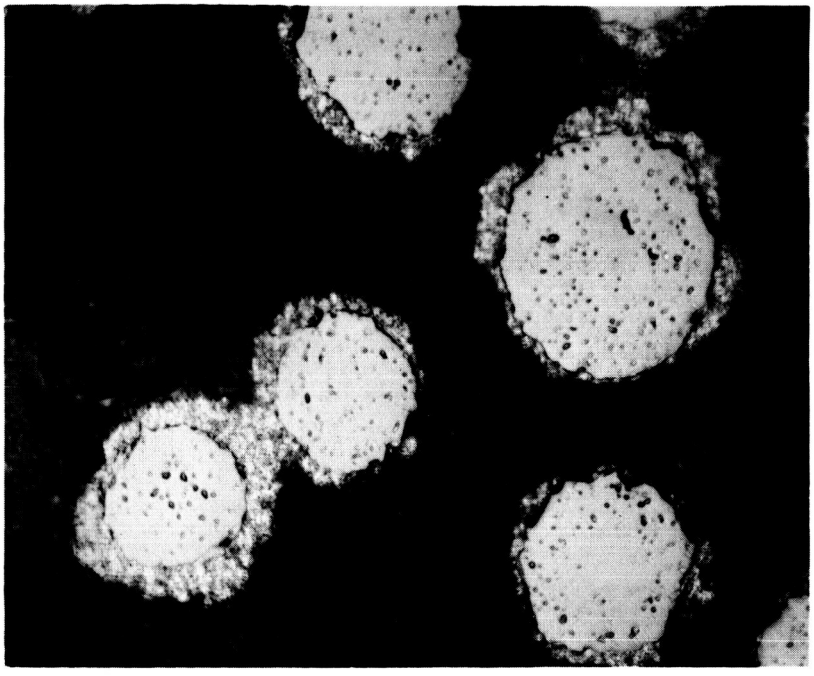

Magn 500X

Fig. 4(a). Thoriated Tungsten Coated Spherical, -270 + 400 Mesh, Uranium Dioxide Particles Containing 28 Volume Percent of Tungsten-4 Volume Percent Thorium Dioxide

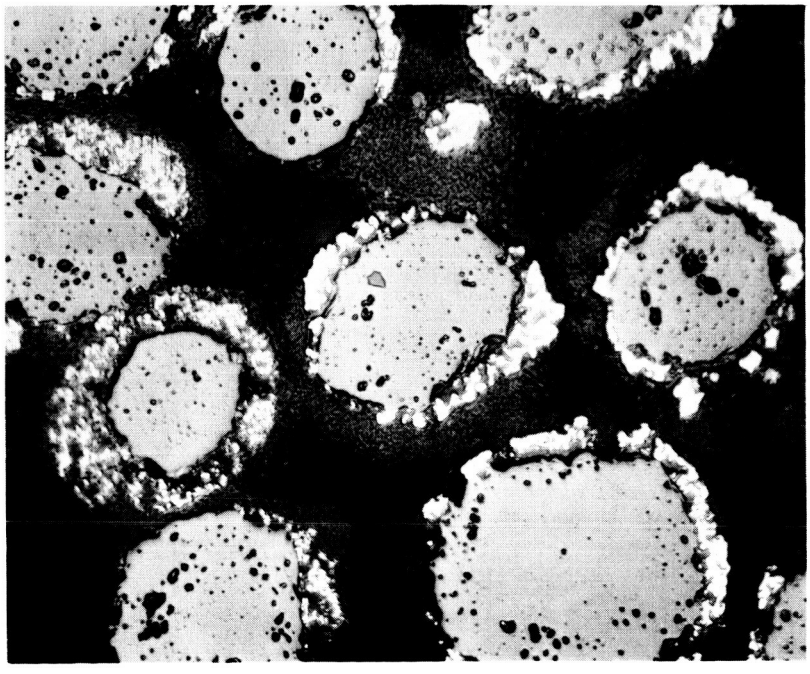

Magn 500X

Fig. 4(b). Duplex Coating of Tungsten and Thorium Dioxide on Spherical, -270 + 400 Mesh, Uranium Dioxide Particles Containing 50 Volume Percent Uranium Dioxide-30 Volume Percent Thorium Dioxide-20 Volume Percent Tungsten

dioxide to determine whether any interference in the polarographic analysis can be introduced by the presence of yttrium oxide or thorium dioxide. In neither case was any interference noted.

The O/U ratio of the uranium dioxide in the uranium dioxide with 33 volume percent yttrium oxide was found to be 2.27 or, approximately 27% of the uranium was present as U (+6).

The O/U ratio of the coprecipitated uranium dioxide-yttrium oxide was determined to be 2.35 or, approximately 35% of the uranium was present as U (+6).

The O/U ratio of the uranium dioxide-thorium dioxide solid solution particles was found to be 2.014. The O/U ratio for this material is expected to be close to 2.00, as there would be little tendency to form a nonstoichiometric oxide from two tetravalent oxides.

A recent report in the literature (Ref. 4) states that uranium dioxide and yttrium oxide reacted in vacuum or in hydrogen at elevated temperatures to form solid solutions which have a strong affinity for oxygen and will oxidize on exposure to air at room temperature. This may account for the formation of high O/U ratios of the uranium dioxide-yttrium oxide solid solutions. Roberts of Harwell reports that the behavior of uranium dioxide-yttrium oxide solid solutions is quite different from uranium dioxide-thorium dioxide solid solutions, as the uranium dioxide-yttrium oxide solid solution contains anion vacancies which fill with oxygen very readly (Ref. 5). The oxidation may proceed at a measurable rate at room temperature, but the reduction to U(+4) may only be accomplished under strong reducing conditions. Oxygen accommodated in vacancies is more tightly bound than oxygen in interstitial sites.

D. FUEL PLATE FABRICATION

The fabrication procedure for preparing the cermet fuel plates used in this investigation is essentially that process developed at NASA-Lewis Research Center (Ref. 6). The process, which is a powder metallurgical process, consists of the following steps:

(1) The tungsten powder and uranium dioxide are weighed to the nearest 0.01 gram. The powders are then dry blended in a standard V-type blender for 45 minutes.

(2) The blended powder is wet mixed with an acetone-stearic acid solution. The stearic acid is equal to 2 weight percent of the powder blend. The powders are dried under a heat lamp in air and then passed through a 60 mesh sieve.

(3) The powder is then placed in a rectangular steel die and leveled with a powder leveling device to achieve a uniform thickness. The powder is then compacted at 9 tsi.

(4) The compacted cores are then stoked into the sintering furnace at a rate of 4 in./hr and are sintered at 1725° C for 16 hours in hydrogen.

(5) The sintered cores are clad on the flat surfaces with 0.0025-inch tungsten foil by wrapping the foil tightly over each core prior to rolling.

(6) The clad core assembly is heated in a hydrogen atmosphere furnace and then hot rolled at 1950° to 2000° C. The composite is rolled to a total reduction of 50% in thickness, using a rolling schedule of 5% reduction per pass.

(7) After rolling, the plates are flattened by applying dead weight to the surface of the plate and reheating the plate to ~1700° C for about 30 minutes. This step is repeated as often as necessary to achieve final flatness.

The program consisted of fabricating two lots of samples. The first lot of samples, which were for Martin-Nuclear testing, consisted of plates incorporating the process variations and fuel modifications as listed in Chapter II of this report. The second lot consisted of samples chosen by NASA after reviewing the fuel loss test results. These samples were fabricated and delivered to NASA. The rolled samples prepared for Martin testing measured ~1 x 3 x 0.020 inches, while the samples shipped to NASA measured ~1-7/8 x 6 x 0.021 inches.

In general, there was little difference in the fabrication characteristics of the various test specimens made under this program, with the exception of those lots containing the fine-particle, ceramic grade uranium dioxide. These specimens exhibited greater sinterability than the others, which resulted in considerably more shrinkage, edge cracking, and warpage during sintering. The average sintered density was ~96% of theoretical as compared to 90% for the standard core and 86% for the cores containing 30 volume percent oxide. These plates also had a greater tendency to produce additional edge cracking during rolling as compared to the other specimens. The yield of acceptable plates for this type was only 50%.

The microstructures of the as-rolled specimens are shown in Figs. 5 through 22. The most significant differences in the structures of the plates is seen in Figs. 10 and 11 of Types III(a) and III(a)1, which contained the fine-particle, ceramic grade uranium dioxide,

and Fig. 12 of Type III(b), which contained the hollow-core uranium dioxide particles. Figures 10 and 11 show the effect of the fine-particle uranium dioxide in acting as a grain refining agent in inhibiting grain growth of the tungsten in the matrix. The hollow-core uranium dioxide, shown in Fig. 12, has undergone considerable densification during the hot rolling operation, and the fuel particles no longer show the hollow-core structure. It is interesting to note that the microstructure of the samples in the as-rolled condition, (rolled at NASA) (see Fig. 6), is somewhat refined as compared to the as-rolled sample shown in Fig. 7 (rolled at Martin-Nuclear). It is believed that this is a result of the different rolling schedules used by the two groups. The NASA schedule utilizes a rolling temperature of ~1900° C, with an average of 5 rolling passes of approximately 10% reduction each. The Martin-Nuclear schedule, as previously noted, utilizes a rolling temperature of ~2000° C with an average of 10 rolling passes of approximately 5% reduction each. It is believed that the increased time at temperature coupled with the strain annealing effect of small reductions with the Martin-rolled samples resulted in the slightly larger as-rolled grain size.

The surface grinding of the Task II, Phase (a) cores prior to rolling did not show any obvious improvement in the clad-to-core bonding (Fig. 8). The only observed advantage in surface grinding was to produce a uniform core thickness, which then resulted in minimizing camber during rolling. The use of a rolling temperature of ~2400° C did not show any obvious change in microstructure as compared to the balance of samples rolled at ~2000° C. The samples rolled at ~2400° C are shown in Fig. 9. It is believed that the lower rolling temperature has a tendency to improve the surface of the samples.

The samples of 30 volume percent total oxide rolled with little difficulty. The yield for samples fabricated in this group approached 75%. These specimens also gave a higher yield of usable sintered cores. It is interesting to note that the photomicrographs of the coated uranium dioxide samples of this group show no visible signs of the coatings after rolling. However, this may indicate a high degree of diffusion of the coatings into the uranium dioxide particle.

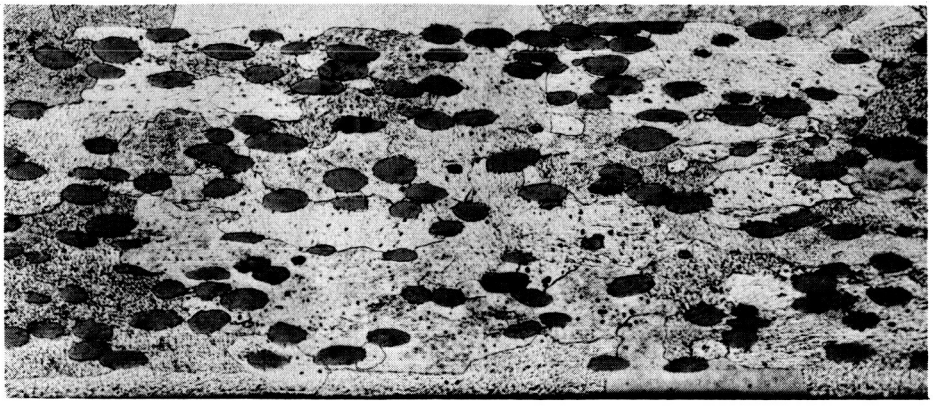

a. As rolled

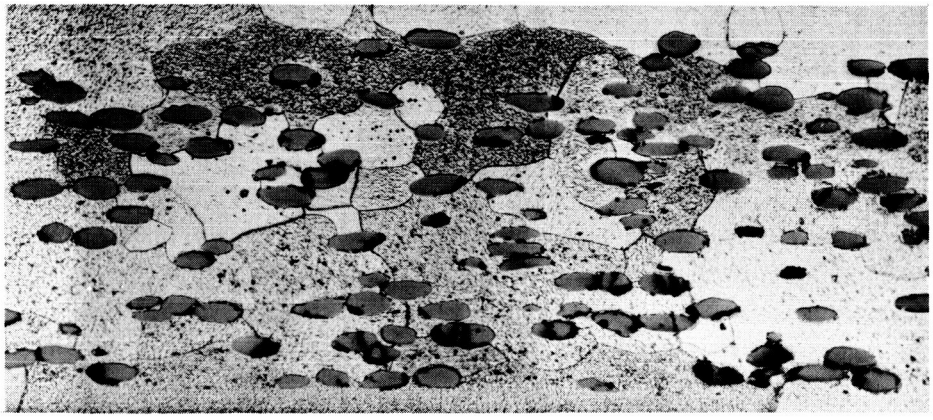

b. After thermal static test 10 hr 4500° F at 10^{-5} torr fuel weight loss 3.1%

c. After 10th thermal cycle test at 4500° F 1/2-hr cycles at 10^{-5} torr fuel weight loss 83.5%

Etchant--Murikami

Magn 100X

Fig. 5. Microstructure of Standard Transverse Sections

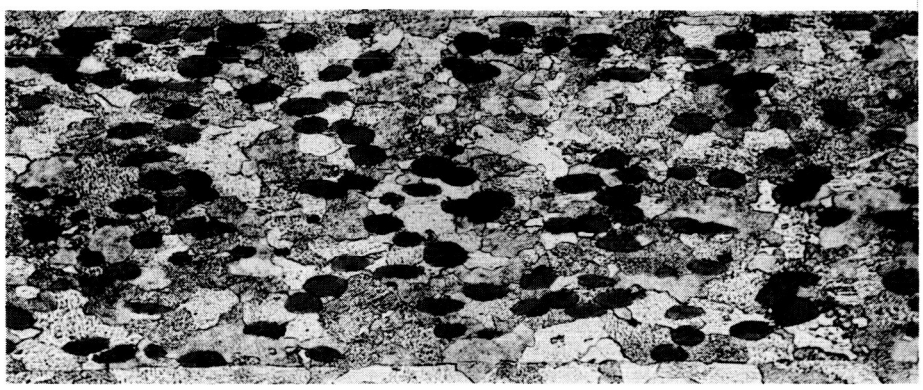

a. As rolled

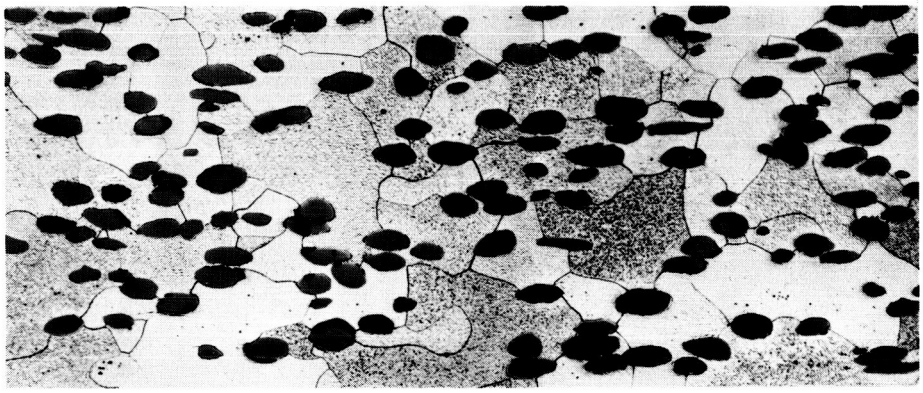

b. After thermal static test 10 hr 4500° F at 10^{-5} torr fuel weight loss 0.8%

c. After 10th thermal cycle test at 4500° F, 1/2-hr cycles at 10^{-5} torr fuel weight loss 95%

Etchant--Murikami

Magn 100X

Fig. 6. Microstructure of Samples from Task I(a)--Transverse Sections, MN material, NASA-rolled

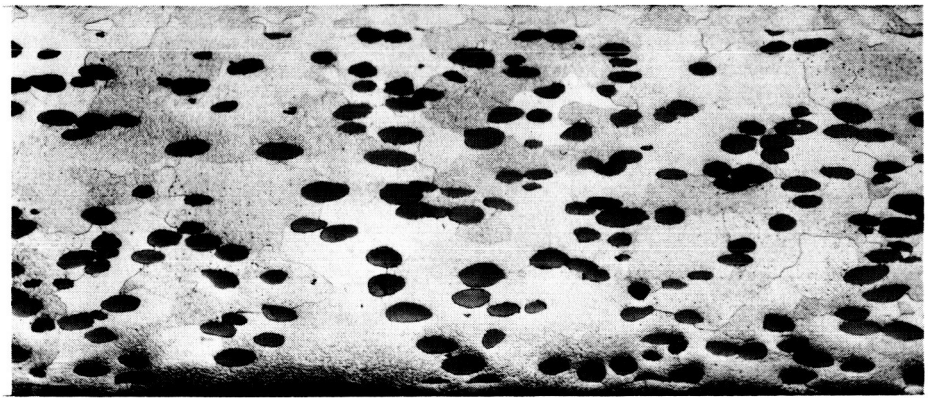

a. As rolled

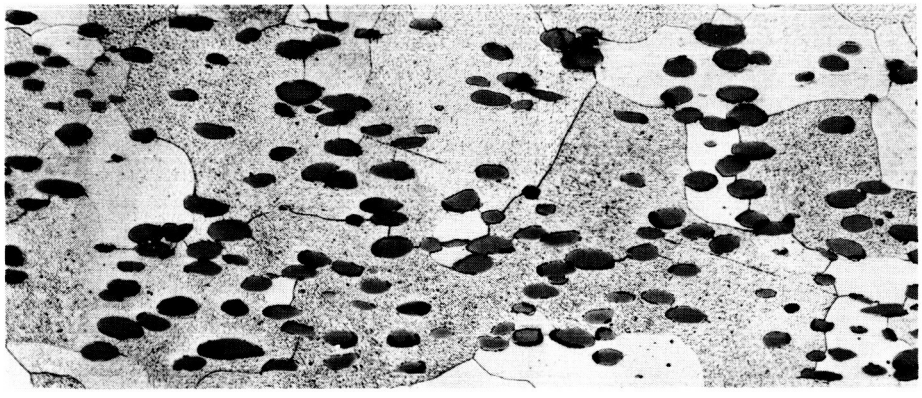

b. After thermal static test 10 hr 4500° F at 10^{-5} torr fuel weight loss 1.3%

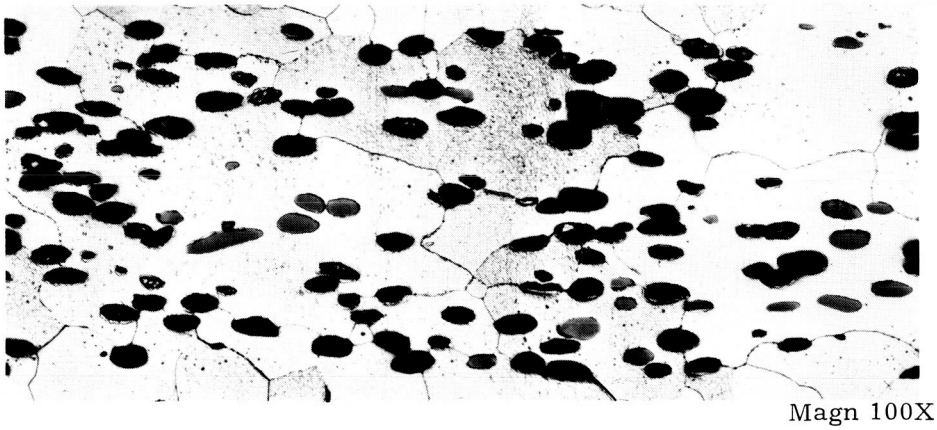

c. After 10th thermal cycle test at 4500° F, 1/2-hr cycles at 10^{-5} torr fuel weight loss 78%

Etchant--Murikami

Magn 100X

Fig. 7. Microstructure of Samples from Task I(b)--Transverse Sections, NASA material, MN-rolled

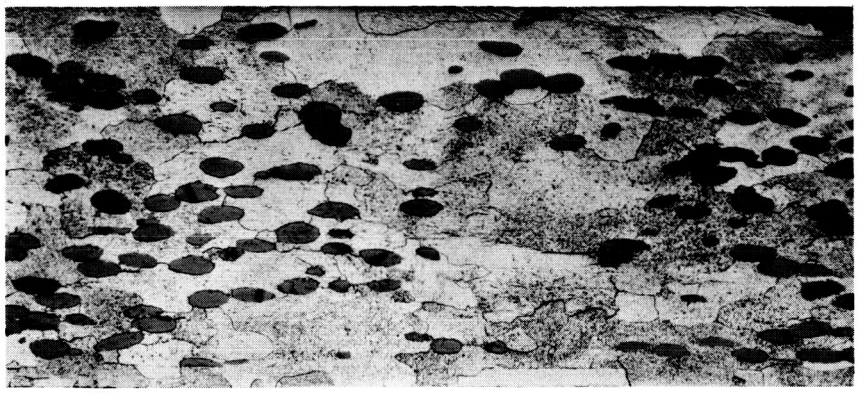

a. As rolled

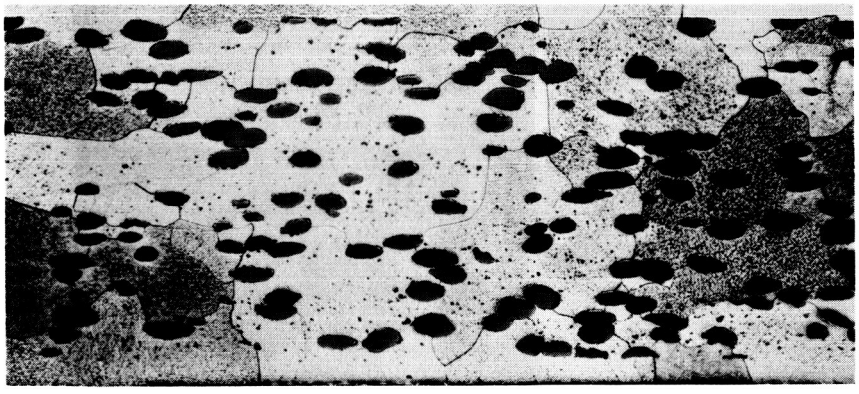

b. After thermal static test 10 hr 4500° F at 10^{-5} torr fuel weight loss 1.1%

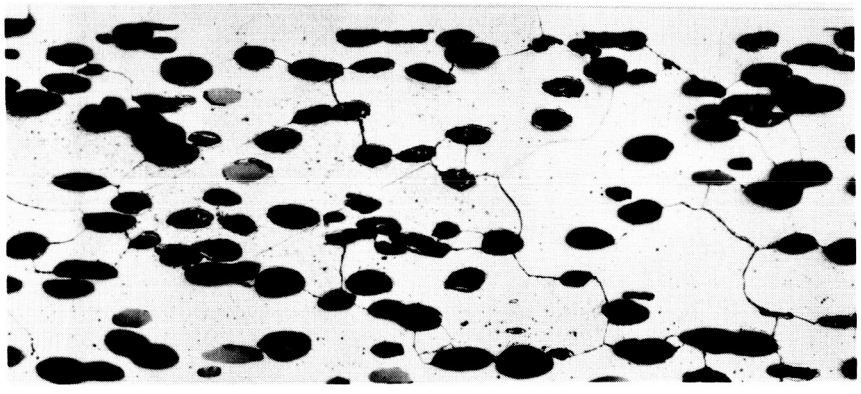

c. After 10th thermal cycle test at 4500° F 1/2-hr cycles at 10^{-5} torr fuel weight loss 92%

Etchant--Murikami

Magn 100X

Fig. 8. Microstructure of Samples from Task II(a)--Transverse Sections, Surface-Ground Cores

a. As rolled

b. After thermal static test 10 hr 4500° F at 10^{-5} torr fuel weight loss 6.9%

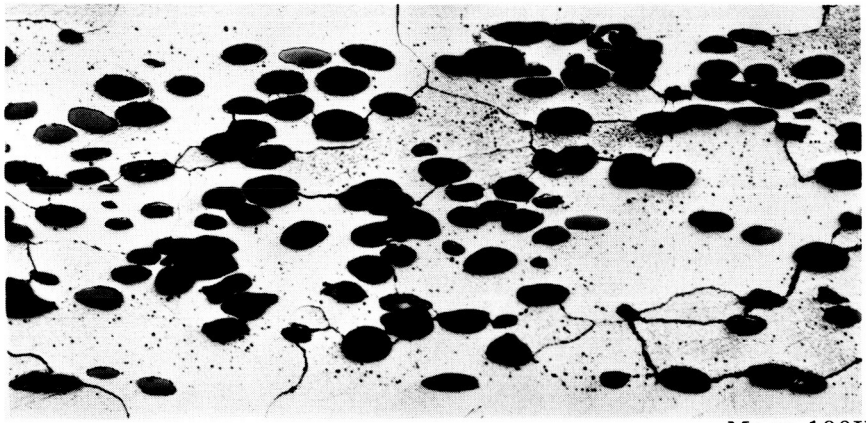

c. After 10th thermal cycle test at 4500° F 1/2-hr cycles at 10^{-5} torr fuel weight loss 88.0%

Etchant--Murikami

Magn 100X

Fig. 9. Microstructure of Samples from Task II(b)--Transverse Sections, High Temperature Rolled (~2400° C)

a. As rolled

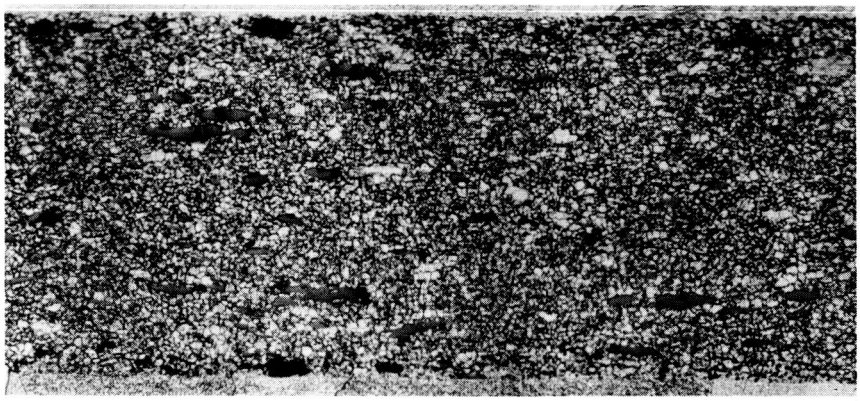

b. After thermal static test 10 hr 4500° F at 10^{-5} torr fuel weight loss 0.8%

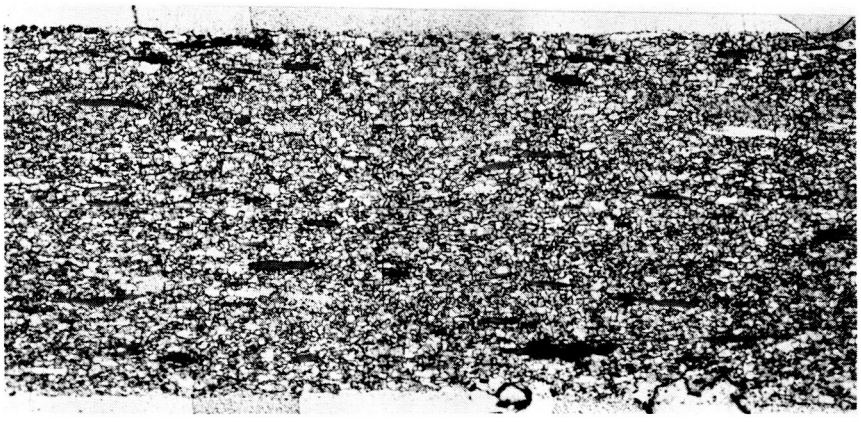

c. After 10th thermal cycle test at 4500° F 1/2-hr cycles at 10^{-5} torr fuel weight loss 5.0%

Etchant--Murikami

Magn 100X

Fig. 10. Microstructure of Samples from Task III(a)--Transverse Sections High Fluorine Fine-Particle Fuel

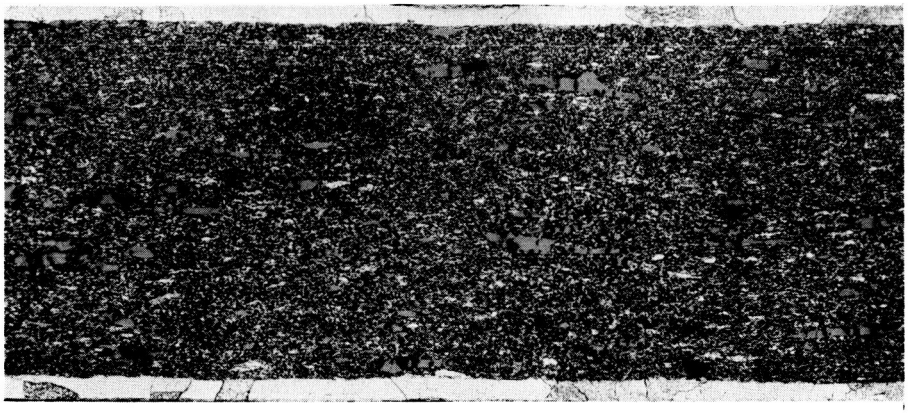

a. As rolled

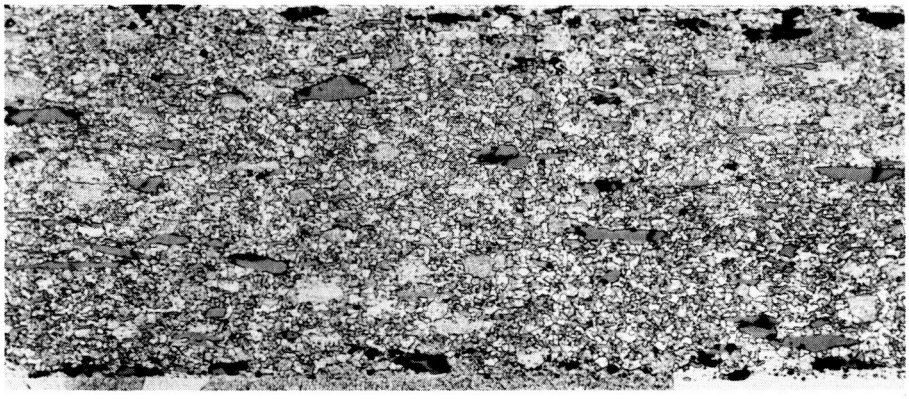

b. After thermal static test
10 hr 4500° F at 10^{-5} torr
fuel weight loss 3.2%

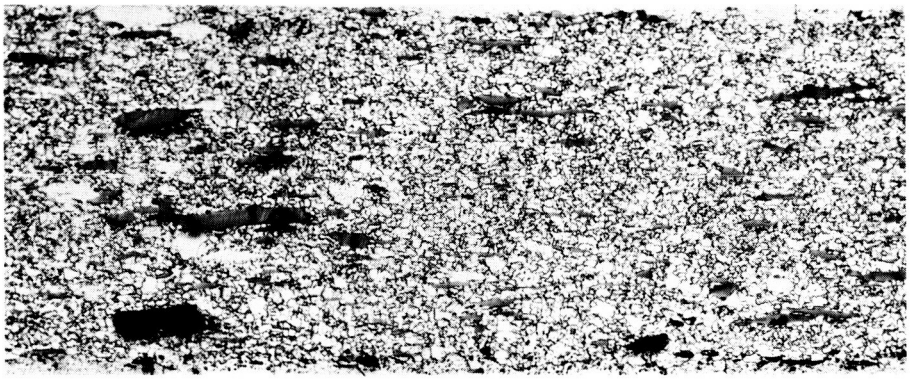

c. After 10th thermal
cycle test at 4500° F
1/2-hr cycles at
10^{-5} torr fuel weight
loss 10.0%

Etchant--Murikami

Magn 100X

Fig. 11. Microstructure of Samples from Task III-a-1--Transverse Sections
Low Fluorine Fine-Particle Fuel

a. As rolled

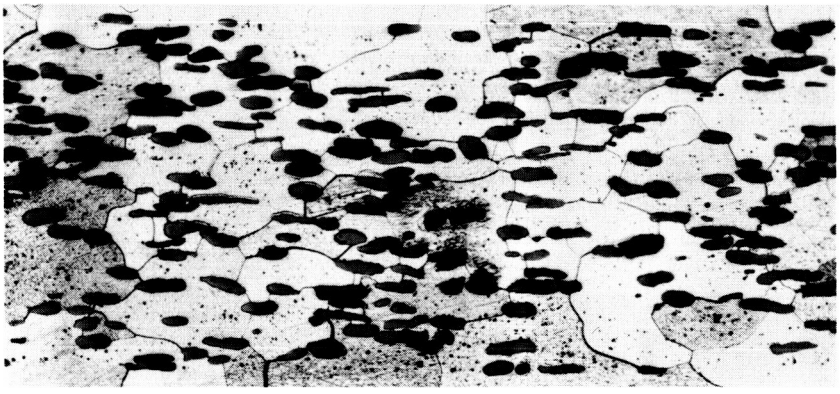

b. After thermal static test 10 hr 4500° F at 10^{-5} torr fuel weight loss 4.5%

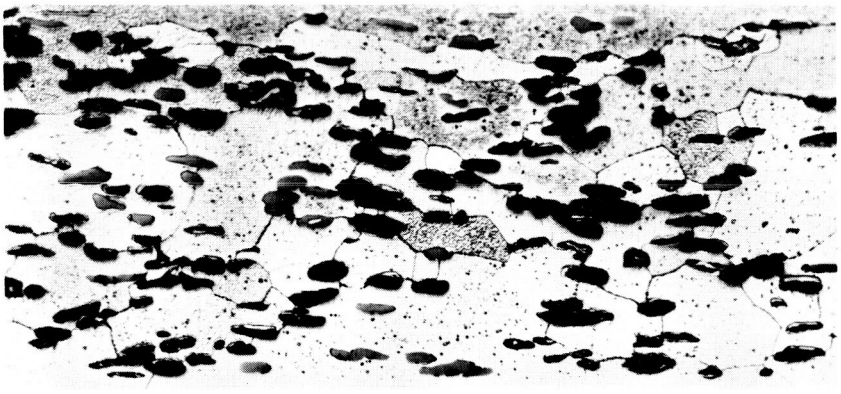

c. After 10th thermal cycle test at 4500° F 1/2-hr cycles at 10^{-5} torr fuel weight loss 93.0%

Etchant--Murikami

Magn 100X

Fig. 12. Microstructure of Samples from Task III(b)--Transverse Sections Hollow-Core Fuel Particle

a. As rolled

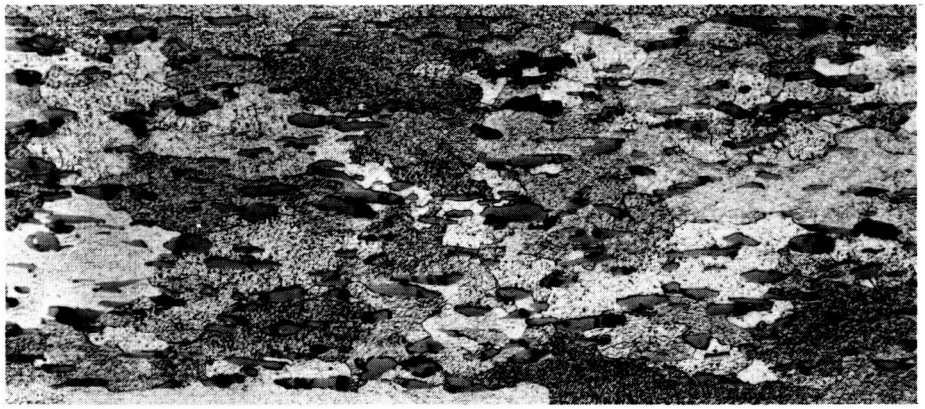

b. After thermal static test 10 hr 4500° F at 10^{-5} torr fuel weight loss 9.5%

c. After 10th thermal cycle test at 4500° F 1/2-hr cycles at 10^{-5} torr fuel weight loss 52.0%

Etchant--Murikami

Magn 100X

Fig. 13. Microstructure of Samples from Task III(c)--Transverse Sections Agglomerated Fine-Particle Fuel

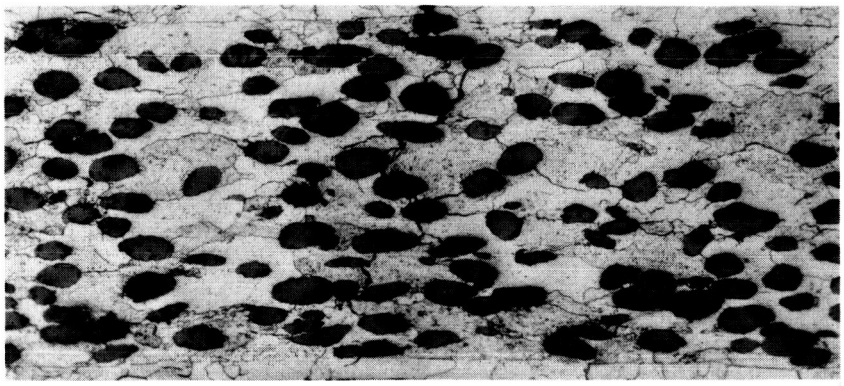

a. As rolled

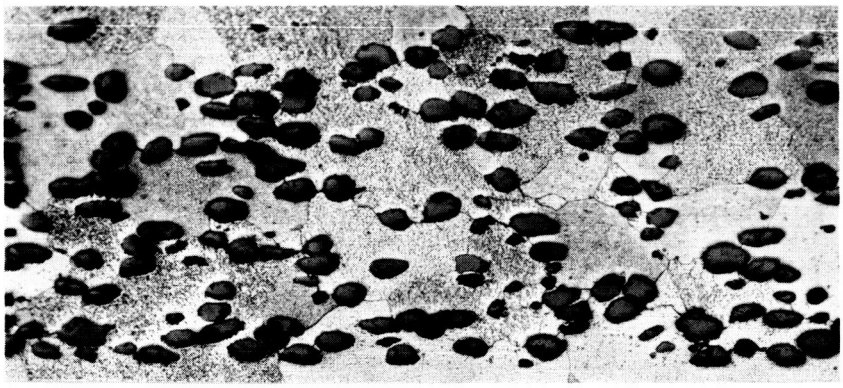

b. After thermal static test 10 hr 4500° F at 10^{-5} torr fuel weight loss 11.4%

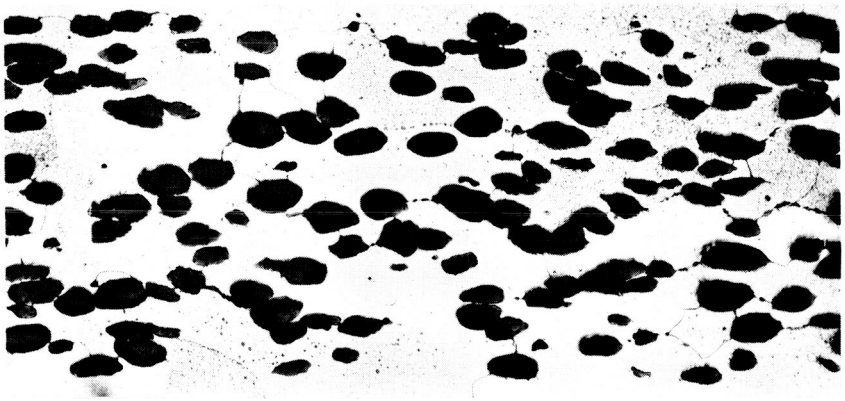

c. After 10th thermal cycle test at 4500° F 1/2-hr cycle at 10^{-5} torr fuel weight loss 11.0%

Etchant--Murikami

Magn 100X

Fig. 14. Microstructure of Samples from Task IV(a)--Transverse Sections Solid Solution of Yttrium Oxide in Uranium Dioxide

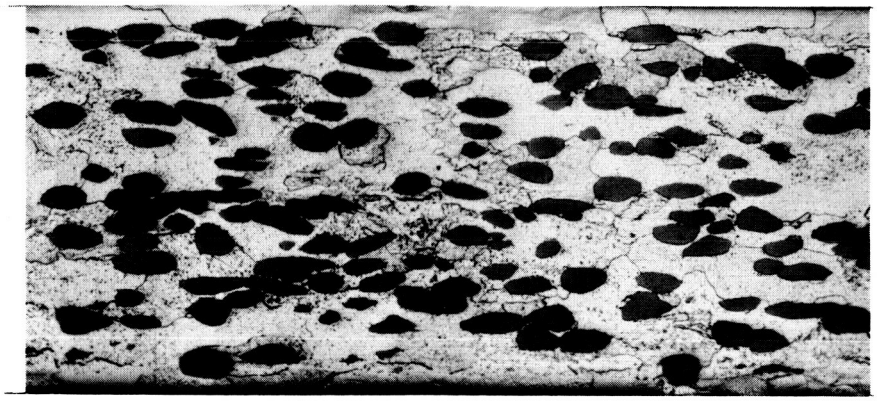

a. As rolled

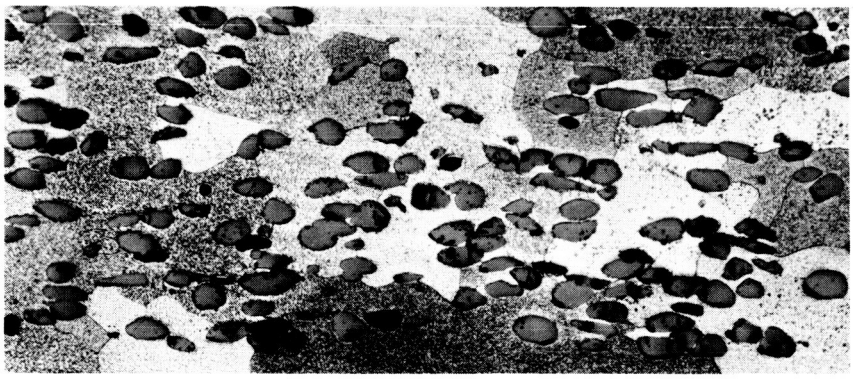

b. After thermal static test
10 hr 4500° F at 10^{-5} torr
fuel weight loss 4.8%

c. After 10th thermal
cycle test at 4500° F
1/2-hr cycle at
10^{-5} torr fuel weight
loss 42.0%

Etchant--Murikami

Magn 100X

Fig. 15. Microstructure of Samples from Task IV(b)--Transverse Sections
Solid Solution of Thorium Dioxide in Uranium Dioxide

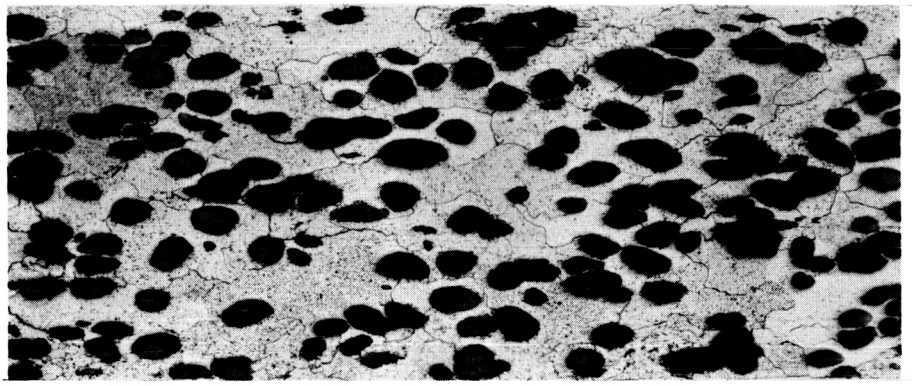

a. As rolled

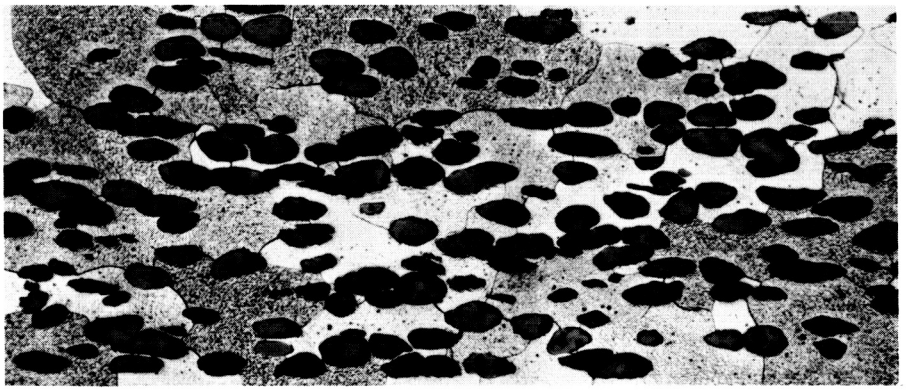

b. After thermal static test 10 hr 4500° F at 10^{-5} torr fuel weight loss 14.8%

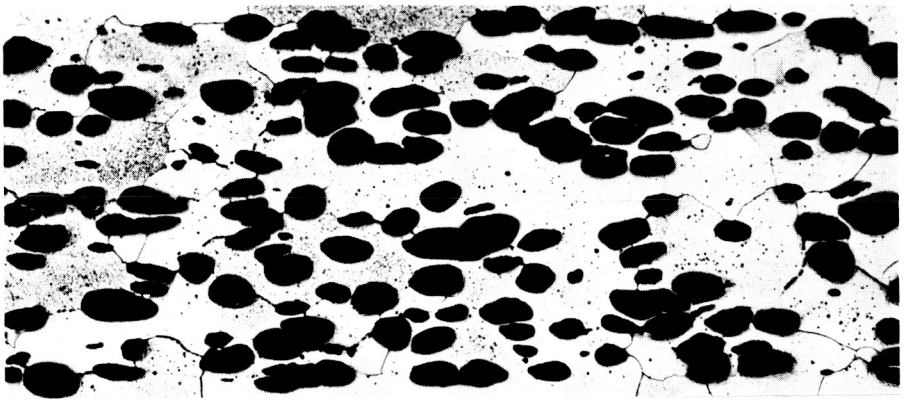

c. After 10th thermal cycle test at 4500° F 1/2-hr cycles at 10^{-5} torr fuel weight loss 16.0%

Etchant--Murikami

Magn 100X

Fig. 16. Microstructure of Samples from Task IV(c)--Transverse Sections Coprecipitated UO_2-UO_3-Y_2O_3

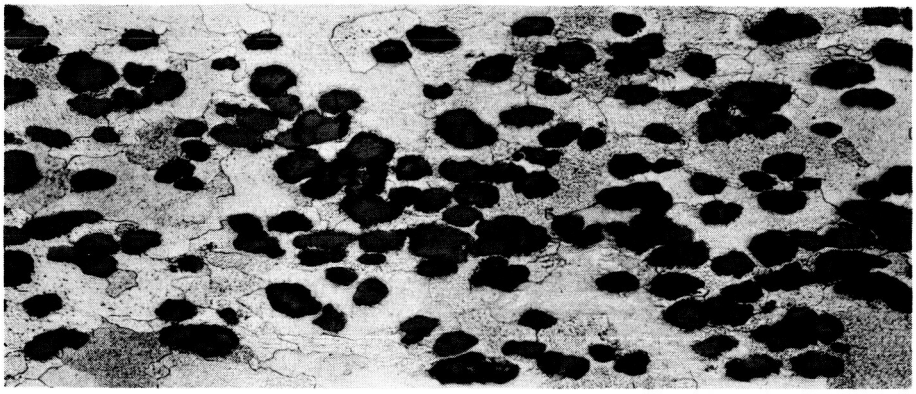

a. As rolled

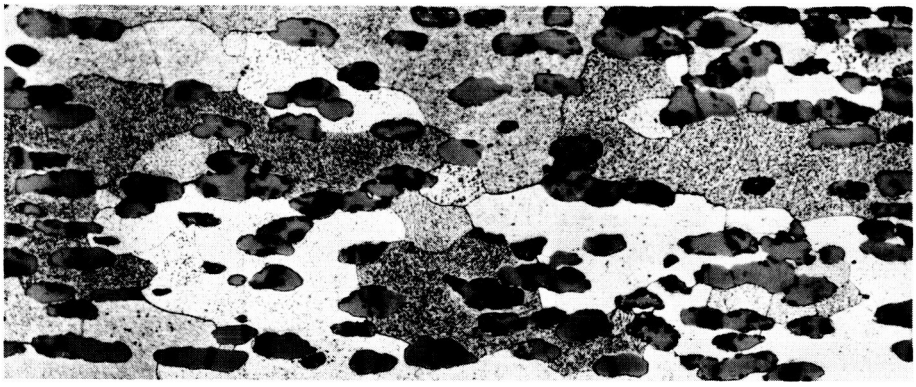

b. After thermal static test 10 hr 4500° F at 10^{-5} torr fuel weight loss 10.3%

c. After 10th thermal cycle test at 4500° F 1/2-hr cycle at 10^{-5} torr fuel weight loss 79.0%

Etchant--Murikami

Magn 100X

Fig. 17. Microstructure of Samples from Task IV(d)--Transverse Sections Coated Fuel Particle with Thorium Dioxide

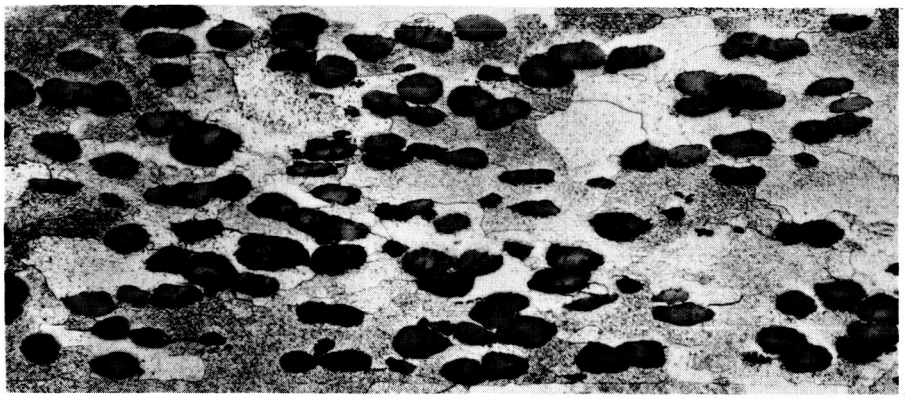

a. As rolled

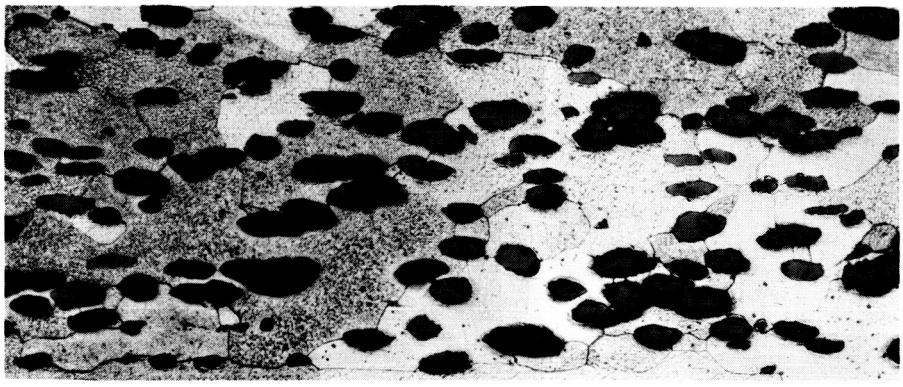

b. After thermal static test 10 hr 4500° F at 10^{-5} torr fuel weight loss 12.9%

c. After 10th thermal cycle test at 4500° F 1/2-hr cycle at 10^{-5} torr fuel weight loss 17%

Etchant--Murikami

Magn 100X

Fig. 18. Microstructure of Samples from Task IV(e)--Transverse Sections Coated Fuel Particles with Yttrium Oxide

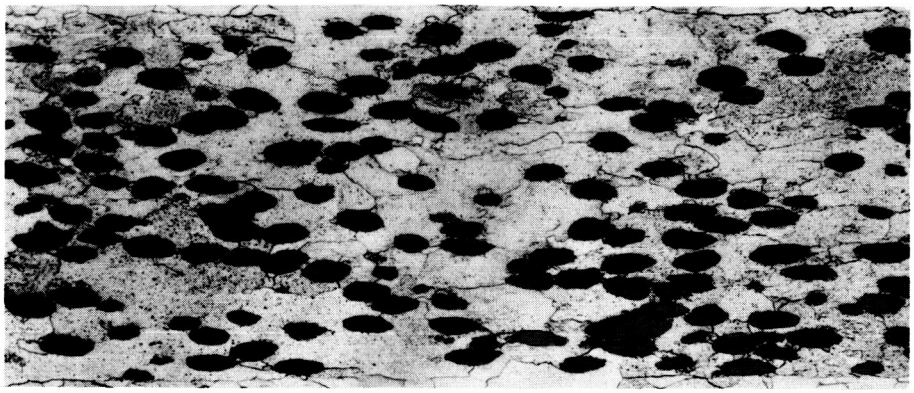

a. As rolled

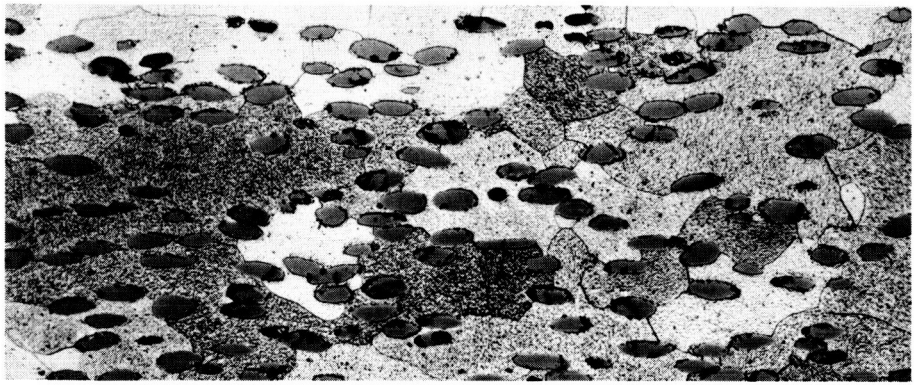

b. After thermal static test 10 hr 4500° F at 10^{-5} torr fuel weight loss 1.3%

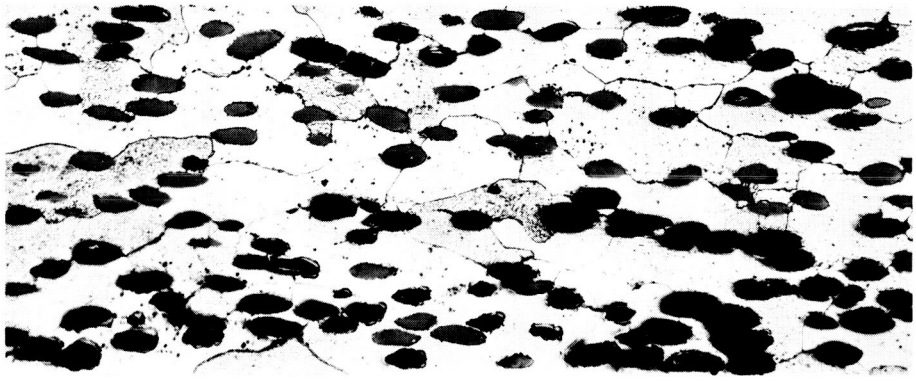

c. After 10th thermal cycle test at 4500° F 1/2-hr cycles at 10^{-5} torr fuel weight loss 58.0%

Etchant--Murikami

Magn 100X

Fig. 19. Microstructure of Samples from Task IV(f)--Transverse Sections, Coated Fuel Particle with Thoriated (2 wt %) W

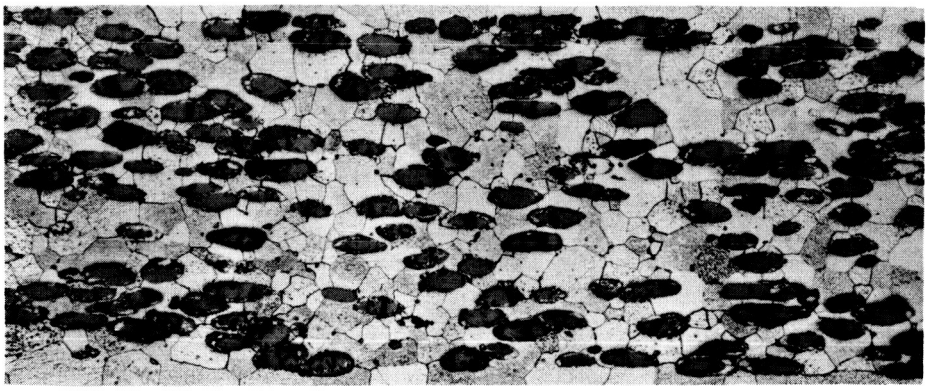

a. As rolled

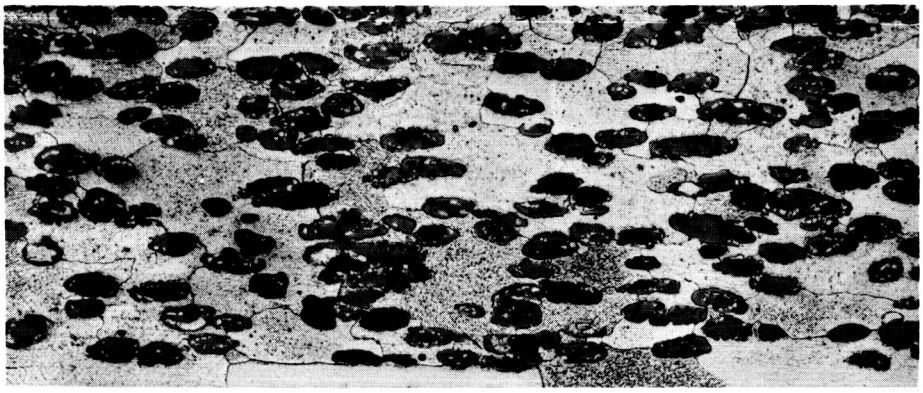

b. After thermal static test 10 hr 4500° F at 10^{-5} torr fuel weight loss 13.7%

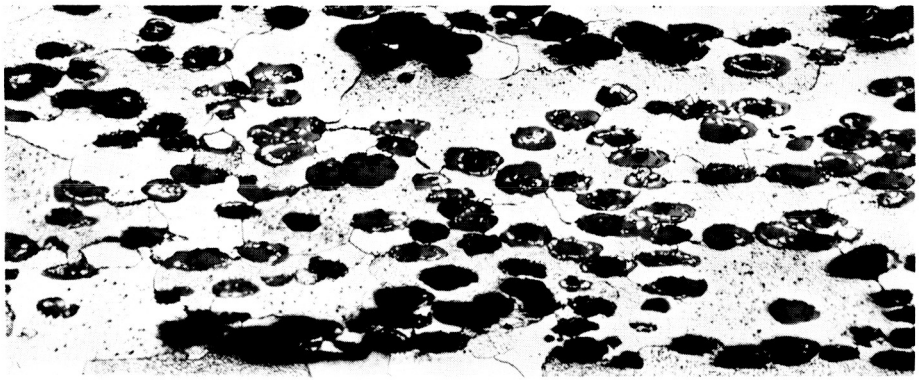

c. After 10th thermal cycle test at 4500° F 1/2-hr cycles at 10^{-5} torr fuel weight loss 79.0%

Etchant--Murikami

Magn 100X

Fig. 20. Microstructure of Samples from Task IV(g)--Transverse Sections, Duplex Coating of W and ThO_2 on Fuel

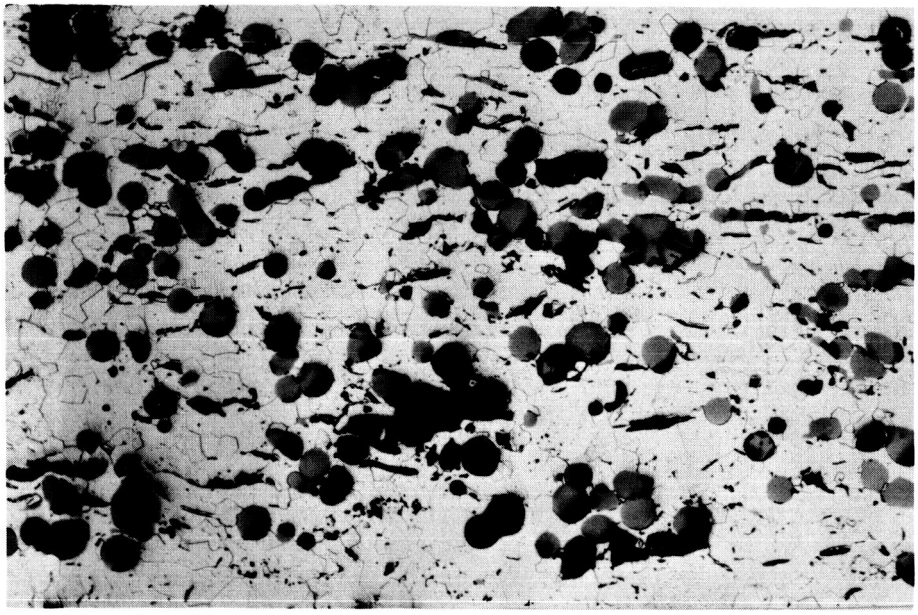

a. Task IV(h)--Sintered plate made from hollow core uranium dioxide

b. Task IV(i)--Agglomerated fuel particle of tungsten and fine particle uranium dioxide

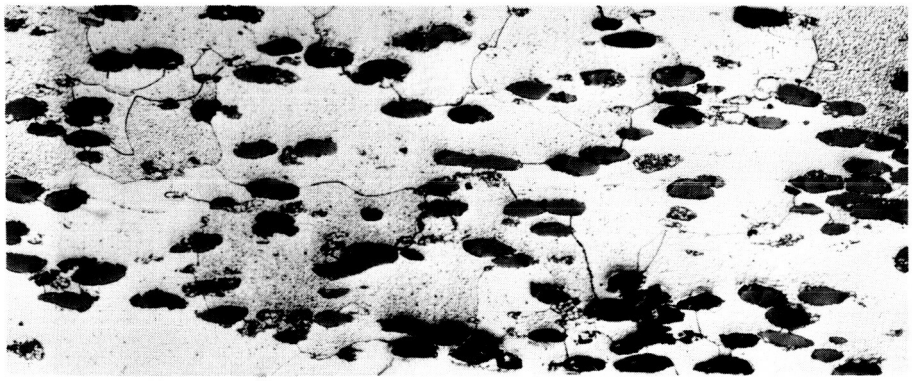

c. Task IV(j)--UO_2 particle coated with thoriated tungsten containing 10 wt % ThO_2

Etchant--Murikami

Magn 100X

Fig. 21. Microstructure of Plate After 4th Thermal Cycle at 4500° F 10^{-5} torr

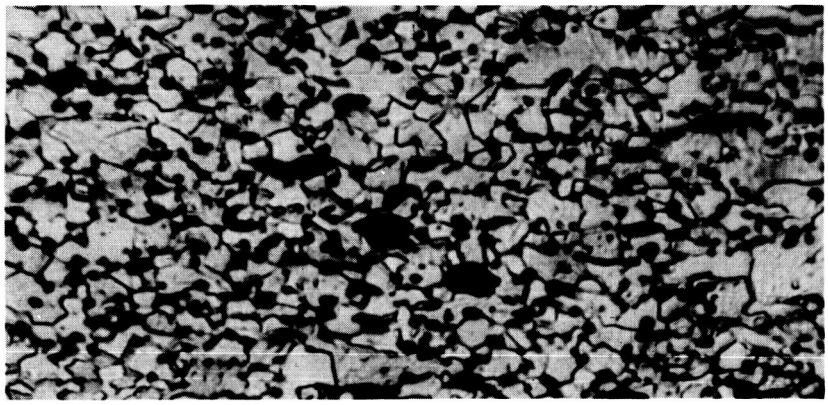

As rolled
Magn 1500X--Murikami's Etchant

Fig. 22(a). Fine-Particle UO_2 Specimen Task III(a)

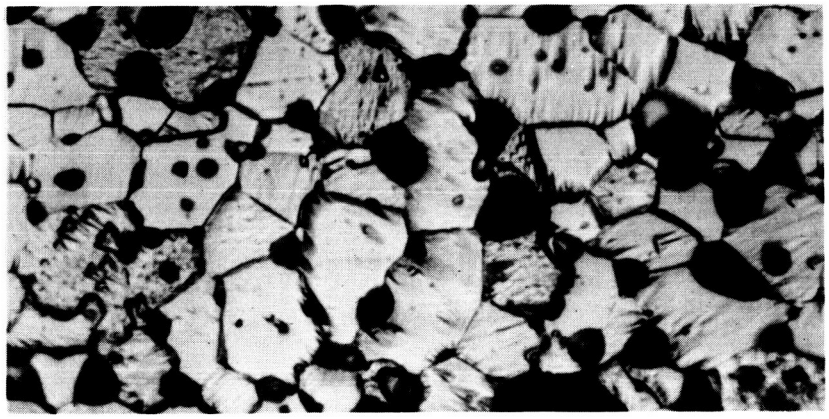

After 10th thermal cycle test at 4500° F 1/2-hr
fuel weight loss 5.0%

Magn 1500X--Murikami's Etchant

Fig. 22(b). Fine-Particle UO_2 Specimen Task III(a)

IV. FUEL RETENTION TESTING

The effect of the physical process and/or fuel composition variations on fuel losses from the cermet fuel elements was determined by subjecting representative specimens of each type to weight loss tests at 2480° C (4500° F) in a vacuum of $< 5 \times 10^{-5}$ torr. The tests consisted of both a static test of 10 hours at 2480° C and a cycle test of 10 thermal cycles from room temperature to 2480° C, with each cycle including a 30-minute hold at the maximum temperature. The test specimens were approximately 1 x 1-1/2 x 0.020 inches, with a total surface area of 3 square inches. Before beginning each test, the test samples were outgassed at 1300° C for one hour in a vacuum of 1×10^{-5} torr. The fuel loss was then determined by a weight loss measurement after each static test or each thermal cycle. The entire weight loss was assumed to be loss of uranium dioxide fuel.

The fuel losses, calculated as percent fuel lost, based on the original fuel loading, are listed in Table 7. The thermal cycling losses are also shown in Figs. 23 to 25. The data presented for the fuel losses represent the average loss shown by two or three test specimens for each specimen type or variable. Although there appears to be reasonable agreement for the test results for each specimen type, the data should be used to indicate a trend rather than for absolute values.

TABLE 7

Weight Loss of Samples After Thermal Testing

		Static Test Loss (%)	Cycle Test Loss After 10th Cycle (%)
I a	MN material, NASA-rolled	0.8	95.0
b	NASA material, MN-rolled	1.3	78.0
II a	Surface-ground cores	1.1	92.0
b	Rolled 2400° C	6.9	88.0
III a	High F fine-particle	0.8	5.0
a-1	Low F fine-particle	3.2	10.0
b	Hollow-core fuel particle	4.5	93.0
c	Agglomerated fine-particle	9.5	52.0
IV a	Solid solution--Y_2O_3 in UO_2	11.4	11.0
b	Solid solution--ThO_2 in UO_2	4.8	42.0

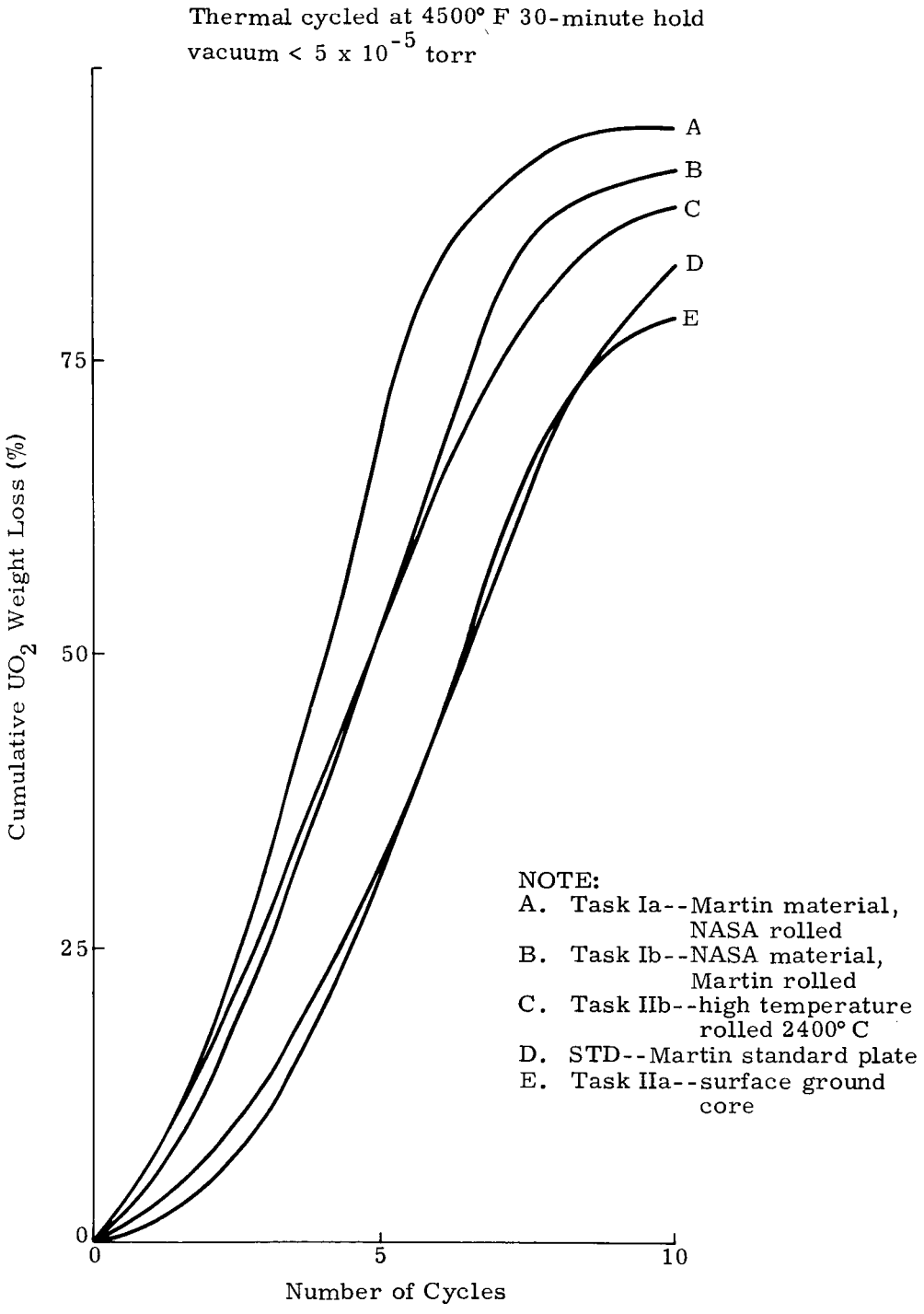

Fig. 23. Fuel Loss Versus Thermal Cycling

Thermal cycled at 4500° F 30-minute hold
vacuum < 5×10^{-5} torr

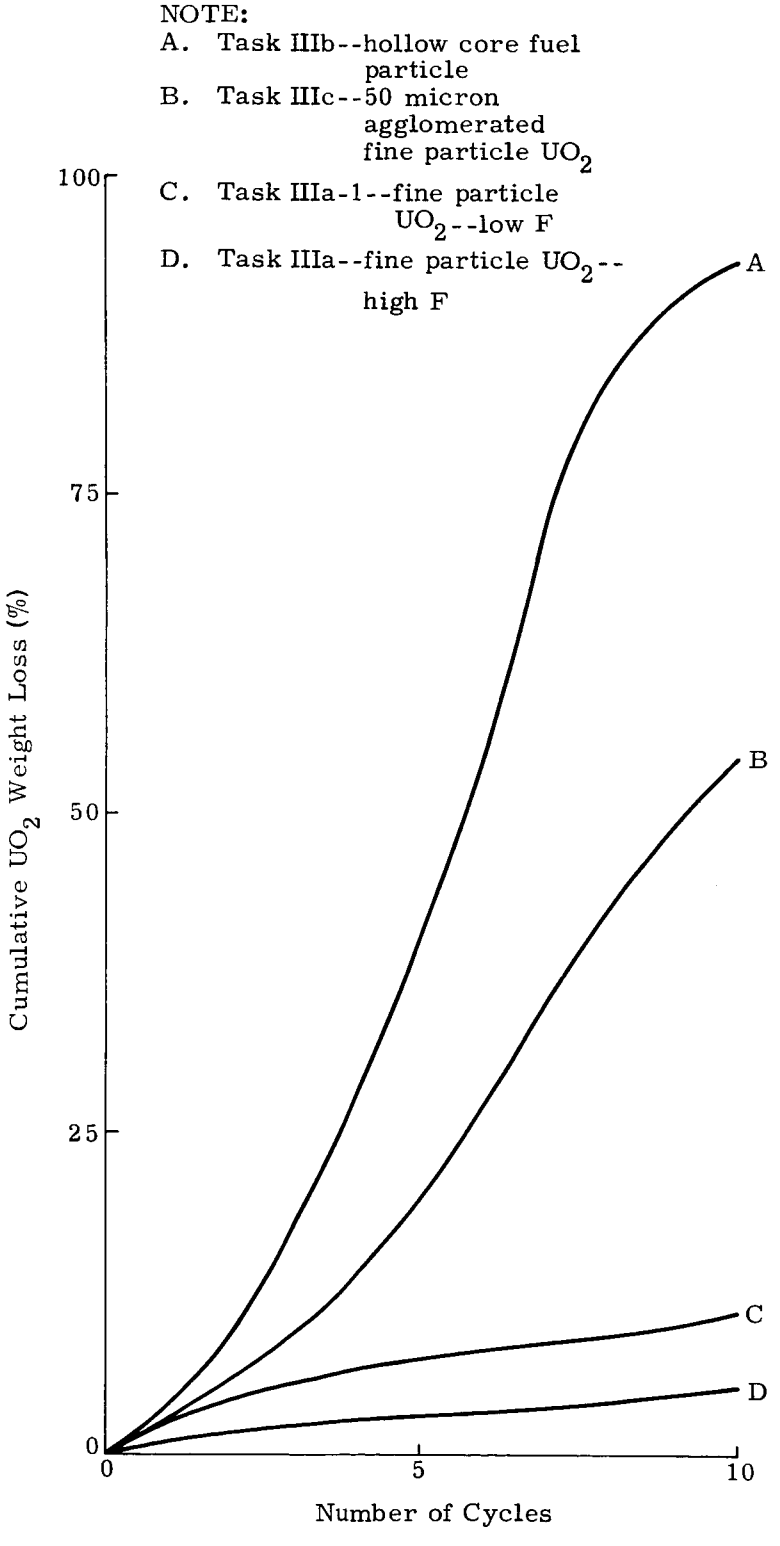

Fig. 24. Fuel Loss Versus Thermal Cycling

Thermal cycled at 4500° F 30-minute hold
vacuum < 5×10^{-5} torr

NOTE:

A. Task IVd--UO_2 particle coated with ThO_2

B. Task IVg--UO_2 particle coated with duplex coating--W + ThO_2

C. Task IVf--UO_2 particles coated with 2% thoriated W

D. Task IVb--Solid solution ThO_2-UO_2

E. Task IVe--UO_2 particle coated with Y_2O_3

F. Task IVc--Coprecipitated Y-U (+6) oxides

G. Task IVa--solid solution Y_2O_3-UO_2

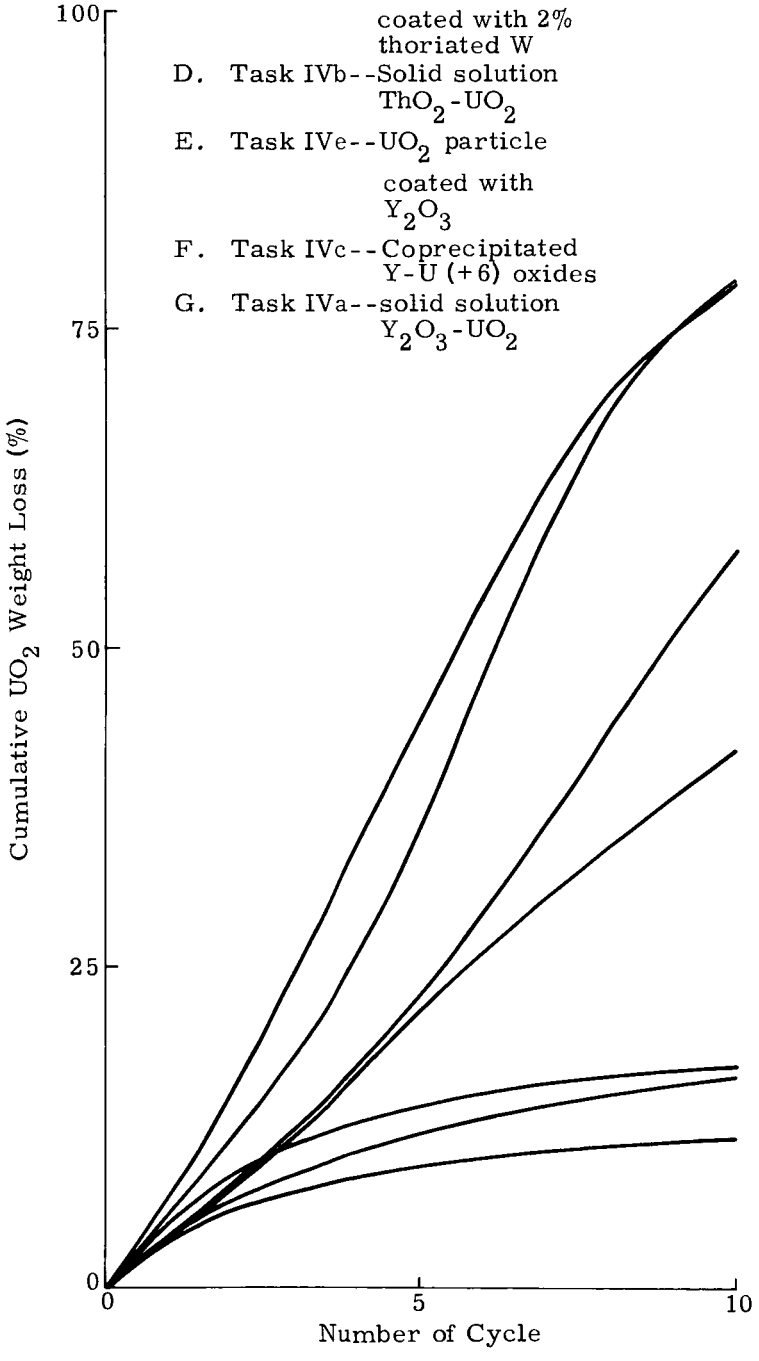

Fig. 25. Fuel Loss Versus Thermal Cycling

TABLE 7 (continued)

		Static Test Loss (%)	Cycle Test Loss After 10th Cycle (%)
c	Coprecipitated UO_2-UO_3-Y_2O_3	14.8	16.0
d	Clad fuel particle with ThO_2	10.3	79.0
e	Coated fuel particle with Y_2O_3	12.9	17.0
f	Coated fuel particle with thoriated W-2 wt % ThO_2	1.3	58.0
g	Duplex coated W + ThO_2 coating	13.7	79.0
h	Sintered plate with hollow-core UO_2		60.3[1]
i	Agglomerated fuel particle of W and fine-particle UO_2		61.6[1]
j	Coated fuel particle with thoriated W-10% ThO_2		42.5[1]
Standard		3.1	83.5

[1]Cycle test loss after 4th thermal cycle

A. STATIC TEST

The static test fuel losses appear to fall into two groupings, i.e., a low fuel loss group (< 5 weight percent) and a high fuel loss group (> 10 weight percent). Essentially the high purity fuel particles (i.e., uranium dioxide with no additive) fell into the low weight loss category. The fabrication process modification (high temperature hot rolling) and the physical modifications to the fuel particles (hollow-core particles and/or agglomerated fines) only served to increase the fuel losses. Almost all of the high fuel loss specimen types were in the Task IV group, which included additions to the uranium dioxide in the form of

oxide solid solutions or oxide coatings. Although the uranium dioxide fuel loading in the Task IV specimens was held constant at 20 volume percent, the addition to the fuel increased the total ceramic content to 30 volume percent. The one specimen type in this group that showed a low static test fuel loss was the specimen containing uranium dioxide coated with thoriated tungsten. The contribution here of the thorium dioxide in the coating was equivalent only to an additional 1 volume percent of ceramic phase.

Photomicrographs of the samples after static test are shown in Figs. 5 through 22. As the fuel losses in the static test samples are low, compared to thermal cycle losses, it is considered that the missing fuel particles shown in the photomicrographs are due primarily to metallographic pull-out during polishing rather than fuel loss during testing. The microstructure of the tungsten matrix had essentially achieved an equilibrium grain size for all samples, with the one exception of the fine-particle uranium dioxide Task III(a) samples. Obviously, this fine-particle uranium dioxide had the same effect in inhibiting grain growth in the tungsten matrix as that found with thoriated tungsten. It is interesting to note that, of the two fine-particle uranium dioxide-type samples fabricated, the samples of lower fluoride content, III(a), contained a greater number of agglomerates. It is believed that the increased number of agglomerates found in these samples was the major reason for the different weight loss found between these two types of fine-particle uranium dioxide samples. One specimen of Type II(b), when tested, showed an exceptionally high fuel loss. Examination of the microstructure of this sample indicated excessive clad cracking, which is believed to be the reason for the high fuel losses.

B. CYCLE TESTING

Of the materials tested, the fine-particle uranium dioxide and the uranium dioxide-yttrium oxide solid solution fuel particles have shown the lowest fuel losses under thermal cycling conditions. Yttrium oxide additions in other forms, as the particle coating and the coprecipitated solid solution particle, have also shown a considerable reduction in fuel losses. The thorium dioxide additions to the uranium dioxide have exhibited a lesser effect in the reduction of fuel losses. The thorium dioxide solid solution additions to the uranium dioxide were more effective in aiding fuel retention than were the thorium dioxide coatings on the fuel particles. The coatings, in general, were not as effective in reducing fuel losses as were solid solution additions. Since the coatings were nonuniform, they did not afford the protection that was anticipated. High purity uranium dioxide particles, i.e., those with no addition, show high fuel losses in the 80 to 95% range, with the exception of the fine-particle, ceramic grade uranium dioxide, whose

fuel losses fall in the 5 to 10% range, and the agglomerated, fine-particle uranium dioxide, which appears to be a compromise between the normal spherical uranium dioxide and the fine-particle uranium dioxide.

Photomicrographs of the samples after cycle testing are shown in Figs. 5 through 22. The high fuel particle losses are apparent in these photographs.

Although it is felt that some uranium dioxide is removed as a result of mounting-polishing pull-outs, the bulk of missing fuel particles is due to fuel loss during the cycling test, as shown by weight loss measurements. Some migration of the fuel in the tungsten grain boundaries can be seen in all samples tested. Figure 22 shows the microstructures of a fuel plate made from the fine-particle uranium dioxide, at 1500X, both in the as-rolled condition and after thermal testing. Although some obvious tungsten grain growth has taken place during testing, the tungsten grain size is still significantly smaller than the other samples tested. A considerable amount of uranium dioxide particle coalescence has also occurred during testing. It is interesting to note that the hollow-core fuel particles shown in Fig. 21(a) have completely densified during the thermal cycle testing. Most of these particles showed a high degree of central porosity in the as-sintered state (see Fig. 1(a)). It is believed that the higher temperature encountered during testing (~ 2500° C) resulted in this further densification.

V. CONCLUSIONS

The low fuel losses experienced during static testing are attributed primarily to edge loss of fuel by vaporization from the unclad edges of the plates. Higher fuel losses were encountered during static testing with the samples which contained the high oxide loading. These samples, primarily of Task IV, contained an additional oxide to the uranium dioxide that was designed to stabilize the uranium dioxide. As a result, the total oxide content of the fuel was increased to 30 volume percent.

It is believed that the high fuel losses encountered on thermal cycling were due primarily to a partial dissociation or reduction of the uranium dioxide at high temperatures to $UO_{2-x}+O$ and to a migration of the fuel and/or its decomposition products through the grain boundaries of the coarse-grained tungsten matrix. Through repeated cycling of the fuel element, the following reactions will take place:

(1) $UO_2 \rightarrow UO_{2-x}+O$ (at high temperature)

(2) $UO_{2-x} \rightarrow UO_2+U$ (on cooling to room temperature).

From above reactions, the reasons for the high fuel losses which were experienced during thermal cycling of the high purity, coarse-particle uranium dioxide are quite apparent.

The best fuel retention properties of the material investigated in this program have been demonstrated by specimens containing fine-particle uranium dioxide with an average particle size of ~1 micron. The effect of the fine-particle uranium dioxide dispersed in tungsten appears to be that of a grain-refining agent. This fine-grained tungsten matrix provides a tortuous path for the escape of fuel, rather than the simple path found in the normal, coarse-grained tungsten matrices. The destructive effect of the difference in thermal expansion between the high-expansion uranium dioxide and low-expansion tungsten is also reduced with the use of finely dispersed oxide fuel particles. In addition to this, it is believed that the increased number of grain boundaries increases the dilution of grain boundary impurities. This effect, in turn, results in making the boundaries less subject to crack propagation. The specimens which contained the fine-particle uranium dioxide showed low fuel losses in both thermal cycle and static tests. The weight loss on cycle testing of these samples was from 3 to 6 times higher than those lost on static test.

Yttria additions to the uranium dioxide have shown a strong stabilizing effect on the uranium dioxide as evidenced by low fuel losses during thermal cycling. The weight losses of these samples during both cycle and static tests were essentially the same. The effect is considered to be a solid solution stabilization effect as the uranium dioxide is "alloyed" with the yttrium oxide whose cation has a lower valency than the U^{+4}. This is probably due to the fact that a cation of lower positive charge, such as Y^{+3}, in replacing a tetravalent ion U^{+4}, will require fewer oxygen ions than the U^{+4} ion, therefore, not filling vacancies and creating a distorted lattice. The replacement of U^{+4} by another cation of +4 valency does not change the oxygen-metal ratio of the system as in the case of uranium dioxide-thorium dioxide solid solutions. Thorium dioxide additions to the uranium dioxide exhibited a lesser effect on fuel retention during thermal cycling.

Tungsten-uranium dioxide cermet specimens were prepared which involved some process modifications in their fabrication. These modifications included modified rolling procedures at different laboratories, hot rolling at higher temperatures (2400° C instead of 2000° C), and surface grinding of the sintered core prior to cladding. No significant reductions in fuel losses under thermal cycling conditions were achieved as the result of any of these modifications

Fuel particle modifications, agglomerated fines, and hollow core spheres also showed high fuel losses under thermal cycling tests.

VI. RECOMMENDATIONS

It is recommended that further investigations be conducted in the following areas.

A. SOLID SOLUTION STABILIZATION OF URANIUM DIOXIDE

A broader scope of solid solution "alloys" of uranium dioxide should be investigated. Oxides that form solid solutions with uranium dioxide should be studied. These oxides should be selected on the basis of cation size and valence. It is also recommended that the effect of various amounts of additives be evaluated to determine the additive level that produces the maximum stabilizing effect and minimum fuel loss.

B. EFFECT OF PARTICLE SIZE ON FUEL LOSSES

A range of particle sizes of uranium dioxide should be prepared and evaluated in the tungsten-uranium dioxide cermet plate. A particle size range of 0.1 micron to 10 microns should be considered and evaluated for cermet plate fabricability, structure, and fuel retention.

C. COMBINED EFFECT OF URANIUM DIOXIDE SOLID SOLUTION IN FINE-PARTICLE SIZE

The effect of a selected uranium dioxide solid solution composition in combination with fine-particle material should be evaluated. If the two effects are cumulative, this would probably result in an extremely low fuel loss material.

REFERENCES

1. Gedwill, et al., "Fuel Retention Properties of Tungsten-UO_2. Composites," prepared for Materials Information Meeting--A.N.L., March 25-26, 1964.

2. ASTM No. 5-0550 Ewanson and Fayat NBS Circular 539, II, 33 (1953).

3. Econ. Geol. 56, 241, (1961).

4. Bartram, et al., "Phase Relations in the System UO_2-UO_3-Y_2O_3, Journal of America Ceramic Society Vol. 47, pp 171-5,1964.

5. Roberts, L.E.J., U.S.-U.K. Conference on Uranium Oxides, June 1959.

6. Watson, Gordon K., Technical Memorandum--Fabrication of Thin Tungsten-Uranium Dioxide Composite Plates, NASA (to be published).

7. McDonald, et al., Technical Memorandum--Fabrication and Retention of UO_2 in Tungsten, NASA TM-X-473, June 1961.

DISTRIBUTION LIST

NASA Lewis Research Center (3)
21000 Brookpark Road
Cleveland, Ohio 44135
Attention: G. Watson

NASA Lewis Research Center (1)
21000 Brookpark Road
Cleveland, Ohio 44135
Attention: Technical Utilization Office, MS 3-16

NASA Lewis Research Center (2)
21000 Brookpark Road
Cleveland, Ohio 44133
Attention: Library

U.S. Atomic Energy Commission (3)
Technical Reports Library
Washington, D. C.

AEC Headquarters (1)
Div. of Reactor Development
Washington, D. C.
Attention: S. Christopher

National Aeronautics and Space Administration (2)
Washington, D. C. 20546
Attention: NPO

NASA Lewis Research Center (1)
21000 Brookpark Road
Cleveland, Ohio 44135
Attention: Office of Reliability and Quality Assurance

NASA Ames Research Center (1)
Moffett Field, California 94035
Attention: Library

NASA Goddard Space Flight Center (1)
Greenbelt, Md. 20771
Attention: Library

NASA Lewis Research Center (1)
21000 Brookpark Road
Cleveland, Ohio 44135
Attention: John J. Fackler
Contracting Officer, MS 54-1

NASA Scientific and Technical Information Facility (6 Reproducible)
Box 5700
Bethesda, Maryland
Attention: NASA Representative

NASA Lewis Research Center (1)
21000 Brookpark Road
Cleveland, Ohio 44135
Attention: Reports Control Office

U.S. Atomic Energy Commission (3)
Technical Information Service Extension
P. O. Box 62
Oak Ridge, Tenn.

National Aeronautics and Space Administration (1)
Washington, D. C. 20546
Attention: G. Deutsch

NASA Lewis Research Center
21000 Brookpark Road
Cleveland, Ohio 44135
Attention: (One copy to each)
Nuclear Rocket Technology Office, MS 54-1
Neal Saunders, MS 105-1
S. Kaufman, MS 49-2
T. Moss, MS 500-309
J. Creagh, MS 500-309
H. Smreker, MS 54-1
A. Lietzke, MS 49-2
G. McDonald, MS 49-2

NASA Flight Research Center (1)
P. O. Box 273
Edwards, California 93523
Attention: Library

Jet Propulsion Laboratory (1)
4800 Oak Grove Drive
Pasadena, California 91103
Attention: Library

NASA Langley Research Center (1)
Langley Station
Hampton, Va. 23365
Attention: Library

NASA Marshall Space Flight Center (1)
Huntsville, Ala. 35812
Attention: Library

Argonne National Laboratory (2)
9700 South Cass Avenue
Argonne, Illinois
Attention: J. Schumar
R. Noland

Oak Ridge Gaseous Diffusion Plant (1)
Oak Ridge, Tenn.
Attention: P. Huber

Battelle Memorial Institute (1)
505 King Avenue
Columbus, Ohio
Attention: E. Hodge

Sylvania Electric Products (1)
Chemical & Metallurgical Division
Towanda, Pennsylvania
Attention: M. MacInnis

United Nuclear Corp. (1)
New Haven, Conn.
Attention: E. Gordon

General Atomic Division (1)
General Dynamics Corp.
P. O. Box 608
San Diego, California 92112
Attention: A. Weinberg

Minnesota Mining & Manufacturing Company (1)
Nuclear Products Department
St. Paul, Minnesota
Attention: J. Ryan

NASA Manned Spacecraft Center (1)
Houston, Texas 77001
Attention: Library

NASA Western Operations (1)
150 Pico Blvd.
Santa Monica, California 90406
Attention: Library

Hanford Laboratories (1)
Richland, Washington
Attention: F. Albaugh

General Electric - NMPO (1)
P. O. Box 15132
Evendale, Ohio 45215
Attention: J. McGurty

Nuclear Materials & Equipment Corp. (1)
Apollo, Pennsylvania
Attention: B. Vondra

Westinghouse Electric Corp. (1)
Astranuclear Laboratory
Box 10864
Pittsburgh, Pennsylvania 15236
Attention: D. Thomas

Union Carbide Corp. (1)
Nuclear Products Dept.
Lawrenceburg, Tenn.
Attention: W. Eatherly

Atomics International Division (1)
North American Aviation
8900 Desota Avenue
Canoga Park, California
Attention: S. Carneglia

General Electric Company (1)
Vallecitos Atomic Laboratory
P. O. Box 846
Pleasanton, California
Attention: Dr. A. Karnoff